Escola de Camins
Escola Tècnica Superior d'Enginyeria de Camins, Canals i Ports
UPC BARCELONATECH

TREBALL FINAL DE MÀSTER

Hydraulic tomography coupled to dissolved oxygen measurements of a managed aquifer recharge system

Treball realitzat per:
Tomàs Benet Lock i Feixas

Dirigit per:
Paula Rodríguez i Escales
Sònia Jou i Claus

Màster en:
Enginyeria ambiental

Barcelona, 28 de setembre de 2022

Departament d'Enginyeria Civil i Ambiental

A malalt que ha de viure, l'aigua li és medicina.

Abstract

Water scarcity is a pressing issue in many regions of the globe, present across all five populated continents. Predictions state that there will be a rise in the number of people afflicted by water scarcity, and the degree to which it is suffered will also worsen. In the face of this, efforts are being devoted to creating solutions which can help guarantee universal access to safe drinking water and sanitation.

A proposed solution is water reclamation, which involves treating wastewater to the extent that it can once more be used without prejudice. There are many ways that water reclamation can be achieved, but currently the most commonly employed methods are costly and energy-intensive. An alternative is Managed Aquifer Recharge coupled to Soil-Aquifer Treatment (MAR-SAT), which combines the innate capability of soil to remove pollutants with its capacity to store water for considerable lengths of time, making it accessible when needed.

To investigate this solution, a pilot-scale test facility has been constructed in the wastewater treatment plant (WWTP) of Palamós (Catalonia, Spain). The work presented here was centred on characterising the hydraulics of one of the artificial aquifer systems via a hydraulic tomography. It was determined that the hydraulic conductivity across the system was uniform, in the range of 10^{0}-10^{1} m d^{-1}, which is in line with the value predicted through its empirical relationship with grain-size, and classifies it as somewhat permeable. It was also possible to map the relative hydraulic connectivity, determining that it was generally good longitudinally, and relatively poor in the transverse direction.

Additionally, one of the key mechanisms behind pollutant attenuation in aquifers is degradation of organic matter via redox reactions. Dissolved oxygen (DO) is the strongest oxidising agent typically available in this context, therefore the DO concentration was monitored at four sites in the aquifer before and during the hydraulic tomography. Anaerobic conditions ([DO] < 1 ppm) were observed across all probed sites, and no clear relationship between hydraulic connectivity and DO behaviour could be elucidated.

Contents

List of figures

List of tables

Acknowledgements

Firstly, I would like to thank my thesis supervisor, Paula Rodríguez, for accepting my request to work with her and offering me such an enriching project, as well as for all her guidance and patience throughout.

I would also like to extend my gratitude to Sònia Jou and Lurdes Martínez for all their help and advice, particularly in the field work carried out in this study.

I thank the members of the Groundwater Hydrology Group of the UPC for welcoming me so warmly and making me feel at home from the very first day. Your companionship during the final step of this master's made the daunting task of completing a thesis project much more enjoyable.

I also want to thank those people who, having started off as my screenmates, briefly became my classmates, and finished as my friends. COVID caused our time sharing a classroom to be far too short, but we'll always have ceviche!

Last, but far from least, I thank my family for their love and support. You are my greatest privilege.

1. Introduction

1.1 Water scarcity

Water is one of the fundamental components necessary for all life on Earth, without which it cannot sustain itself. Humans are no exception to this, and as such, in 2010 the UN General Assembly declared access to clean water and sanitation a basic human right (UN News, 2010). This access must be sufficient (50-100 L per day), safe (free from microorganisms, chemical and radiological hazards), accessible (within 1,000 m of the home and collection time must only take up to 30 min), and affordable (cost less than 3% of household income).

The official figures for that same year, 2010, showed that 884 million people did not have this right guaranteed to them (OHCHR, 2010), though the report acknowledged that the real number was, in fact, significantly higher due to those living in informal settlements that were unaccounted for.

In order to address this, "access to water and sanitation for all" is stated as one of the Sustainable Development Goals (SDGs), also designed and promoted by the UN (A/RES/70/1, 2015). A host of targets have been created to achieve this overarching goal, which range from guaranteeing safe drinking water, to providing access to sanitation and hygiene, to protecting and restoring water-related ecosystems. The targets most relevant to the work presented here are the following:

> 6.3: Improve water quality, **wastewater treatment** and **safe reuse**, halving the proportion of untreated wastewater and substantially increasing recycling and safe reuse globally by 2030.
>
> 6.4: Increase water use efficiency and ensure freshwater supplies, ensure sustainable withdrawals and **supply of freshwater to address water scarcity** and substantially reduce the number of people suffering from water scarcity.

It is estimated that 80% of our global wastewater flows back to the natural water systems without any treatment, compromising the drinking water of millions with faecal matter and the infectious diseases it causes, such as polio, typhoid, cholera, and dysentery (UN-Water, 2017). The consequences are dire: 1.32 million people died prematurely in 2017 alone due to the consumption of unsafe water (Jeffrey D. Stanaway *et al.*, 2018), almost all of which occurred in sub-Saharan Africa, South and South-East Asia.

Moreover, global freshwater use increased dramatically during the 20th century, from 671 billion m3 in 1901 to 3.86 trillion m3 in 2001, *i.e.* a factor of almost 6 (Ritchie and Roser, 2017). This is primarily associated with population growth, which created a rise in demand for domestic and agricultural uses, and the development of industry, which is also heavily dependent on water. The rise in freshwater use is one of the causes behind the steady decrease in volume of renewable freshwater resources, that is, river flows and groundwater from rainfall (Figure 1).

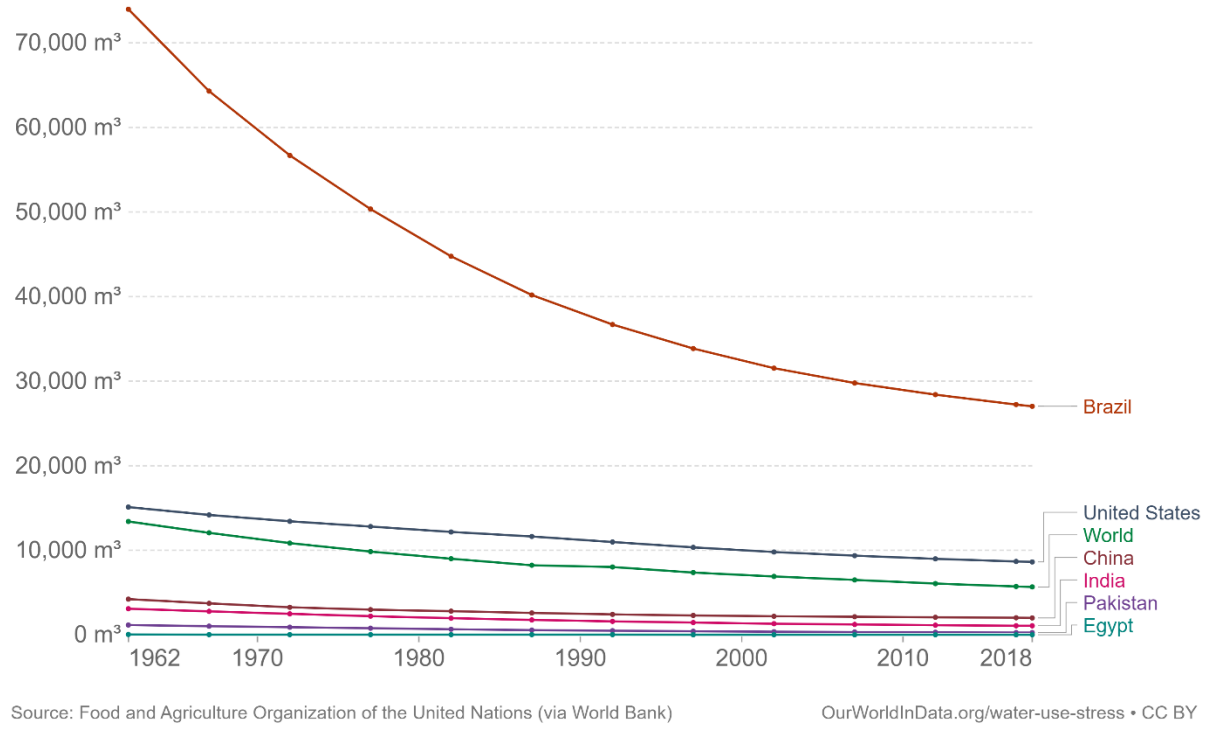

Figure 1. Renewable freshwater resources per capita, 1962-2018 (Ritchie and Roser, 2017).

The higher levels of freshwater withdrawal and lower levels of freshwater resources combine to produce greater water stress, itself defined as a ratio of the two. While high water stress does not necessarily imply immediate water scarcity, it does indicate that the use of freshwater is not sustainable, which if not addressed will ultimately lead to scarcity. Water stress and scarcity do not currently affect everyone across the globe equally, but they are present across all continents, and certain countries and regions are deeply afflicted by them (Figure 2).

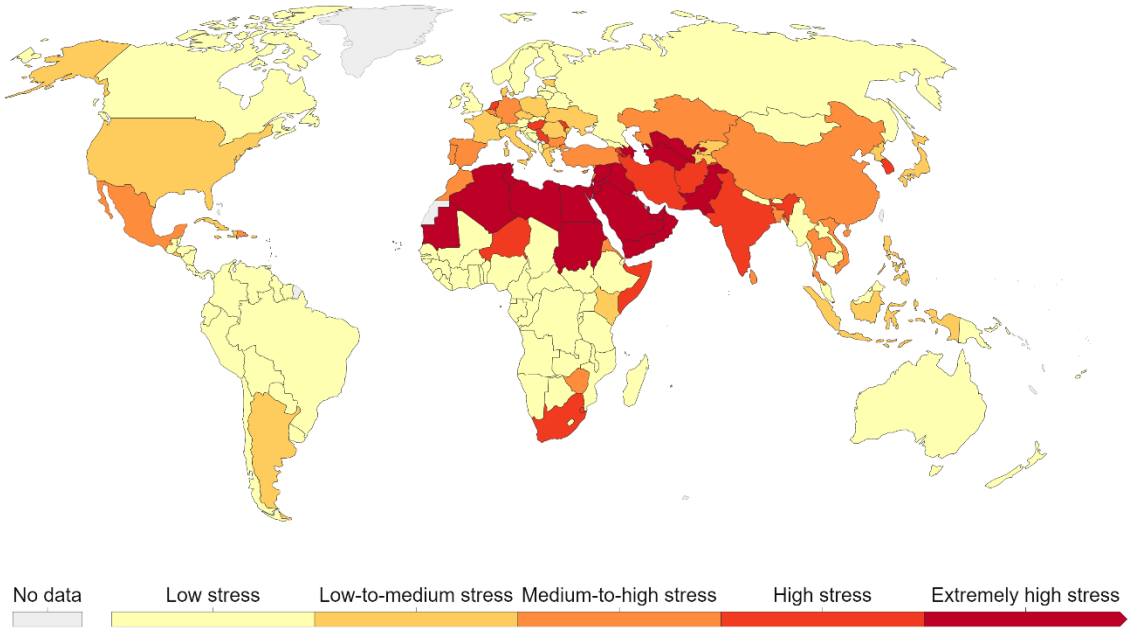

Figure 2. Freshwater withdrawals as a share of internal resources in 2017. The water stress categories are defined as follows: if withdrawals are < 10% of resources, the stress is low; 10-20% is low-to-medium stress; 20-40% is medium-to-high stress; 40-80% high stress; and > 80% is extremely high stress (Ritchie and Roser, 2017).

The number of people and regions suffering from water stress and scarcity is predicted to increase, and the degree to which it is suffered to worsen. The major reasons behind this are well-known: a growing population, particularly in urban areas of low-income countries, and climate change. The urban centres of low-income countries are the most rapidly growing populations in the world (UN-Habitat, 2022), which is placing a sudden and unprecedented pressure on the water bodies surrounding them, both for domestic consumption and for agriculture. In addition, the latest IPCC report states that the warmer climate is changing the water cycle across the globe (Gulev *et al.*, 2022). Higher surface temperatures will drive up evapotranspiration over land, worsening drought events. Some of the regions projected to experience more severe and frequent drought episodes are South-Western South America, Western North America, and the Mediterranean Basin. Rainfall patterns are also changing, becoming less predictable: the interannual variability in precipitation will become greater than the seasonal variability, complicating the tasks of forecasting and planning.

Catalonia, where the study presented in this work was carried out, lies on the north-western shore of the Mediterranean Sea. As such, one does not need to look far in space or time to perceive the effects described above. The territory experienced a significant drought event this past summer, despite receiving relatively normal levels of precipitation in comparison to recent years (Bernis, 2022). The very high temperatures during May, June, July, and August

(over 8 °C higher than the reference period of 2009-2020 in June, and over 6 °C higher in July and August), caused both greater water consumption and higher levels of evapotranspiration, leading to critically low levels of water stored in the reservoirs scattered across the territory. This crisis has left powerful images of parched ground where normally sizeable water bodies host many aquatic activities (Figure 3).

Figure 3. Image of the reservoir *la Llosa Del Cavall*, in Solsonès county, at 30% capacity. Taken in August of 2022 (Rabadà).

Confronted with this reality, it is clear action must be taken to preserve this most precious of resources and maintain sustainable levels of it. There are many open fronts dealing with the issue, but the one which will be the subject of the present work is water reclamation, specifically in the form of managed aquifer recharge coupled to soil-aquifer treatment.

1.2 Water reclamation

Water reclamation, also known as water reuse and water recycling, is the practice of treating water obtained from various sources, often wastewater or stormwater, to a sufficient quality to meet the standards required for use. Depending on said use, the standards are more or less stringent, and consequently the treatment more or less intensive.

Reclaimed water can have a variety of uses, from agricultural irrigation, to cooling towers in industry, to irrigation of golf courses. Some even consider that the water sourced downstream for potable usage is an indirect form of water reclamation, since a significant portion of that water is comprised of treated effluent from upstream wastewater treatment plants.

One noteworthy use for reclaimed water is managed aquifer recharge (MAR). MAR has been defined as "the intentional recharge of water to aquifers for subsequent recovery or environmental benefit… both quantity and quality [must be] managed effectively" (Dillon *et al.*, 2019), with an aquifer being a geological formation through which water can travel due to its pores or fractures. Such an operation can be especially valuable in the Mediterranean region, which is densely populated and has a considerable demand for water, and more so given the current and foreseen water scarcity context described in section 1.1.

Since it is vital to ensure that the water used to recharge aquifers is not harmful to the underground environment, or to possible end-users after the water has been recovered, this procedure comes with the drawbacks of being expensive and requiring large amounts of energy. Various instances of MAR can be found in Catalonia, such as the use of effluent from the Prat de Llobregat WWTP to manage and prevent seawater intrusion (AMB, no date). However, the water used for recharge is first treated with reverse osmosis or ultrafiltration in order to guarantee its quality (ACA, no date). This is the only reclaimed water to undergo such advanced treatment, the rest does not go beyond the disinfection step. Therefore, this also makes it the costliest and most energy intensive form of reclaimed water.

Nevertheless, the ground itself as a porous medium is a natural filter of water, a quality that has led to the development of soil-aquifer treatment (SAT). Partially treated wastewater is used to recharge aquifers, whereupon the levels of pathogens, chemical contaminants, nutrients, and organic matter are substantially attenuated through biodegradation and sorption processes (Maliva, 2020). The degree of pre-treatment will vary depending on the "sources of reclaimed wastewater, recharge methods, location, and, more importantly, public acceptance" (Asano and Cotruvo, 2004). A combination of MAR-SAT could be an interesting solution which addresses both Target 6.3 and 6.4 of the SDG 2030 Agenda.

1.3 MAR-SAT test facilities

A major issue for modern wastewater treatment is the host of recalcitrant components present in wastewater, such as pharmaceutical and hygiene products, microplastics, antibiotic-resistant bacteria and genes. All these compounds are known collectively as contaminants of emerging concern (CECs). Since current treatments are not capable of degrading them, they are released into the environment as part of wastewater treatment plant (WWTP) effluent. The relative novelty of the problem entails that much information on the effects, extent, threshold values, even basic regulation, is still lacking (Trager, 2021). When it comes to MAR-SAT systems, there is a fear that these pollutants could contaminate previously clean groundwater and compromise important drinking water sources. It is therefore vital that techniques be developed and proven which effectively degrade these pollutants, producing clean water that can be safely stored in aquifers without risking contamination.

In view of this, a MAR-SAT test facility was constructed in the Llobregat Basin (Catalonia, Spain), in which a permeable reactive layer was placed on the bottom of an infiltration basin (Valhondo *et al.*, 2014, 2015). This installation has produced largely favourable results, with significant reduction in levels of multiple CECs, however, the authors have noted that the processes that cause this reduction are limited by poor mixing between the recharged water and the native groundwater, as it precludes their respective solutes coming into contact. Indeed, in porous media, mixing is mainly driven by mechanical dispersion and molecular diffusion (Tartakovsky, 2010), both of which are too slow for the purpose of timely pollutant attenuation.

To enhance mixing, some in the field have proposed using engineered injection-extraction (EIE) to induce so-called chaotic advection. The concept involves performing a series of injections and extractions from piezometres to generate transient velocity fields characterised by highly complicated particle trajectories (Bagtzoglou and Oates, 2007), effectively stretching and folding the solute plume, in other words, to increase the volume occupied by the fluid. Theoretical work based on numerical modelling shows promising results (Lester *et al.*, 2010; Piscopo *et al.*, 2013; Rodríguez-Escales *et al.*, 2017), but demonstration through field work is scarce (Cho *et al.*, 2019).

Given this gap in knowledge, another pilot project was established in the WWTP of Palamós (Catalonia, Spain). Six independent recharge systems were built, each coupled to a reactive barrier intended to improve the attenuation of recalcitrant pollutants in WWTP effluent via a MAR-SAT system (Valhondo *et al.*, 2020; Valhondo, Mart & Wang, 2020). Furthermore, two of the tanks were designed specifically for performing chaotic flow experiments. The rationale

behind the project is to study the effectiveness of the barriers, the porous media of the aquifer itself, and of induced chaotic advection, in the fate of CECs.

1.4 Hydraulic tomography

In order to accomplish the goals just described, it is paramount to first understand the hydraulic behaviour of the system being tested. Hydraulic tomography is a technique employed to characterise the hydraulic parameters of aquifers, namely transmissivity, T, hydraulic conductivity, K, and storativity, S, and this is done by performing cross-hole pumping tests (Neuman, 1987; Gottlieb and Dietrich, 1995; Butler Jr. *et al.*, 1999; Yeh and Liu, 2000). Cross-hole refers to the fact that a series of pumping tests are carried out in several piezometres, and the hydraulic head is simultaneously monitored across various observation piezometres. The advantage of this technique is that it produces reliable estimates of the spatial variation in hydraulic conductivity across the section of aquifer that is studied, in contrast to older techniques, which only provide point measurements (Butler Jr., 2005).

Hydraulic conductivity is the ease with which a fluid can move through a medium (m d^{-1}), which, in the case of unconsolidated sediment, occurs through its pores. Transmissivity describes the overall fluid transmission capacity of an aquifer, expressed in units of m^2 d^{-1}, and is also defined as the product of hydraulic conductivity and saturated aquifer thickness, b:

$$T = K \cdot b \tag{1}$$

Given a confined, homogeneous aquifer (constant K) and uniform saturated thickness (constant b), transmissivity will be the same throughout the aquifer. However, if either of these properties change, the capacity of the aquifer to transmit fluid will be affected. For example, if conductivity decreases there will be more resistance to water flow, or if the aquifer thickness shrinks there will be a smaller volume of permeable ground for the water to travel through, both cases cause transmission of water to decline.

The origin behind the hydraulic conductivity of a porous medium is the presence and interconnectivity of pores, or interstitial sites, between the grains that constitute the aquifer. The total porosity, Φ_t, of a given volume of aquifer is defined as the volume taken up by the pores divided by the total volume:

$$\Phi_t = \frac{V_p}{V} \tag{2}$$

This parameter, however, is not what determines the hydraulic conductivity; for that, one needs the effective porosity, Φ_e. It differs from the total porosity in that it only takes into account the so-called "effective volume", that is, the volume of pores that are interconnected and therefore allow fluid to flow. Media such as clay have high total porosity because they contain many small interstitial sites and can therefore hold significant volumes of water. However, they have low effective porosity because the connections between these sites are exceedingly small and exhibit tremendous degrees of tortuosity, which strongly impedes the flow of fluid, and causes clay media to be labelled aquitards rather than aquifers.

The quantity which is actually determined in a hydraulic test is the effective transmissivity, T_{eff}, which is the integrated value of all local transmissivities in the section of aquifer that is probed. Consequently, for a given aquifer, a pumping test carried out with multiple observation piezometres will all yield drawdown curves with roughly the same gradient, reflecting the fact that the quantity being estimated is the effective transmissivity. It also bears mentioning that, even in homogeneous aquifers, the exact conductivity of water is variable to a significant degree even within a small space, and therefore it is not sensible to assign too high a degree of precision (Sánchez-Vila and Batista, 2009).

The coefficient of storativity is a dimensionless parameter which describes the capacity of an aquifer to store or release water, formally defined as the volume of water stored or released per unit change in hydraulic head, over a unit area of the aquifer:

$$S = \frac{\Delta V_w}{A \Delta h} \tag{3}$$

Conversely to transmissivity, the estimated value of storativity (S_{est}) for each observation piezometre, given the same pumping test, will tend to vary greatly. The physical information it provides is the degree of connectivity between the pumping and observation piezometres: the lower the value, the greater the connectivity.

Ascertaining these parameters allows one to predict the behaviour of the groundwater flow, and consequently the advective transport of dissolved species in the groundwater.

1.5 The role of dissolved oxygen

The biodegradation of CECs is highly dependent on reduction-oxidation (redox) conditions, quantified as the redox potential, Eh. In the context of wastewater, the organic contaminants are electron donors (reducing agents), which is why the presence of electron acceptors, *i.e.*, a positive potential, is crucial. The spatial transition between oxic (> 400 mV), sub-oxic (100-

400 mV), and anoxic (< 100 mV) conditions in the vadose zone depends on the availability and relative concentrations of these electron acceptors (Reddy *et al.*, 1998). Furthermore, there exists a well-established hierarchy in the preferred electron acceptor based on the energetic yield of its redox reaction with the organic contaminant, which is: O_2, NO_3^-, Mn(IV), Fe(III), SO_4^{2-}, HCO_3^-, and N_2 (Champ *et al.*, 1979). This confirms the particular importance of dissolved oxygen in soil and groundwater, and is corroborated by multiple studies on microbially-mediated oxidation of organic matter (Bauer *et al.*, 2009; Rolle and Le Borgne, 2019). The latter is precisely one of the key processes involved in SAT, hence expanding our knowledge on the fluctuations of dissolved oxygen concentration in groundwater will aid in understanding the performance of SAT systems.

Elucidating the behaviour of oxygen in soil and groundwater is complex as it is influenced by several processes. Depending on the conditions, diffusion can cause the atmosphere to be either source or sink of soil and groundwater oxygen (Haberer *et al.*, 2012; Borer *et al.*, 2020; Ahmadi *et al.*, 2022). Precipitation brings oxygen-enriched water, and microbial respiration consumes oxygen and therefore depletes it; colder temperatures raise concentrations due to greater oxygen solubility (Massmann *et al.*, 2006) whereas warmer temperatures cause both greater evaporation and favour microbial respiration (Greskowiak *et al.*, 2006).

1.6 Thesis objectives

Given the relevance of aquifer hydraulics and dissolved oxygen in the effectiveness of soil aquifer treatment of wastewater, the goal of this master's thesis is to characterise an artificial aquifer which simulates a MAR-SAT system and evaluate the evolution of the dissolved oxygen concentrations during a set of pumping tests. To achieve this goal, a hydraulic tomography was performed in the pilot system in Palamós, while simultaneously monitoring the levels of dissolved oxygen. The specific objectives are defined as follows:

1. Determine the hydraulic characteristics of the pilot MAR-SAT system and obtain information regarding the hydraulic connectivity between different points.
2. Ascertain what effect, if any, the pumping tests have on the levels of dissolved oxygen in the groundwater.
3. Establish if there are any correlations between the levels of dissolved oxygen, including any changes produced by pumping, and the hydraulic connectivity determined via the first objective.

The execution of this study aims to be a small contribution towards the timely achievement of targets 6.3 and 6.4 of the SDGs, described in section 1.1, and through them the 2030 Agenda as a whole.

2. Methodology

2.1 Site description

The experiments described in this work were conducted on one of the pilot-scale artificial aquifer systems located in the WWTP of Palamós, a town on the north-eastern coast of Catalonia (Figure 4).

Figure 4. Map of Catalonia with the location of Palamós indicated (left), and close-up of the placement of the WWTP within the area it is responsible for (right).

The wastewater undergoes pre-treatment, primary treatment (sedimentation), and biological secondary treatment (activated sludge), then is released as effluent into the Mediterranean Sea via a marine outfall (ACA, 2022).

The system used for the experiments is one of six situated adjacent to one another, designated Tank 1. It is 15 m long, 2.38 m wide, and excavated 1.5 m into the ground (Figure 5) and composed of fine sand (0.1-0.2 mm grain size). Given this characteristic granulometry, one can estimate a total porosity ≈ 40-50% and effective porosity ≈ 20-30%, which predicts that the hydraulic conductivity will be on the order of 1 m d^{-1} (Custodio and Llamas, 1983), on the threshold between poor and good aquifer.

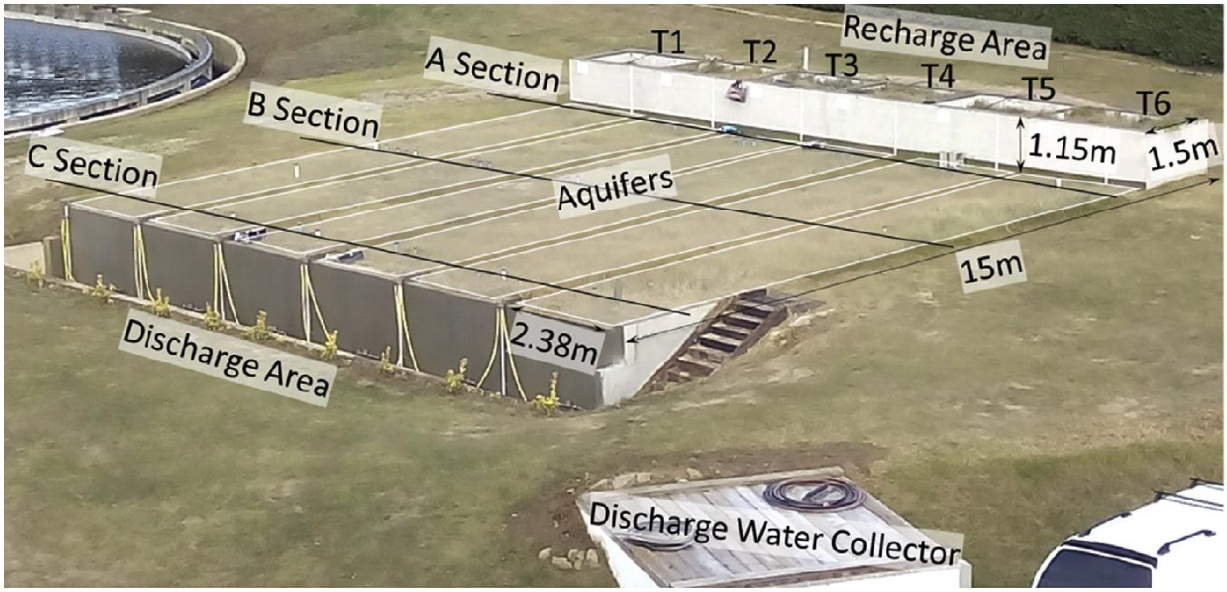

Figure 5. View of the artificial aquifer systems (Valhondo *et al.*, 2020).

At the top end of the aquifer, a 1.5 x 2.38 x 1.15 m^3 structure sits above it and mimics an infiltration basin. This basin constitutes a reactive barrier composed of plant-based compost blended with sand (49% each), with the remainder made up of clay. The role of the reactive barrier is to enhance the degradation of pollutants contained in the wastewater through different mechanisms; the plant-based compost provides sorption sites for uncharged particles and releases dissolved organic carbon (DOC), whereas the clay offers sorption sites for charged particles due to its high ion exchange capacity. The sand provides structural integrity and high hydraulic conductivity.

The discharge point is situated at the opposite end of the artificial aquifer. The space has been excavated to simplify operations such as sampling and manipulation of the hydraulic head. The latter is done by setting the elevation of the discharge pipe through which all of the water exits the aquifer: the lower it is set, the greater the hydraulic gradient.

The hydraulic head was monitored in seven locations across the tank using screened piezometres (PVC 2″) designated as follows: A3, B1, and C1; and BCP1, BCP2, DCP1, and DCP2 (figures 6 and 7). The letters refer to the section of the aquifer in relation to its distance from the edge of the tank: A, B, C, and D are 3, 8, 14, and 11 m away, respectively (note that section D is closer than section C). The 'CP' suffixed in the designation of the second group refers to the fact that those piezometres are intended for upcoming chaotic flow experiments (*chaotic point*), and have screen lengths of 0.4 m. The ordinary piezometres, on the other hand, have screen lengths of 0.1 m. Finally, the numbers designate the distance from the base of the tank at which the piezometres are placed. In the case of the ordinary piezometres, 1, 2, and 3 are placed 0.1-0.2,

0.6-0.7, and 1.1-1.2 m above the base, respectively, while the *chaotic point* piezometres, 1 and 2 are placed 0.1-0.5 and 0.7-1.1 m above the base, respectively. In other words, piezometres named 1 are placed deepest within the aquifer, and those named 3 are placed shallowest.

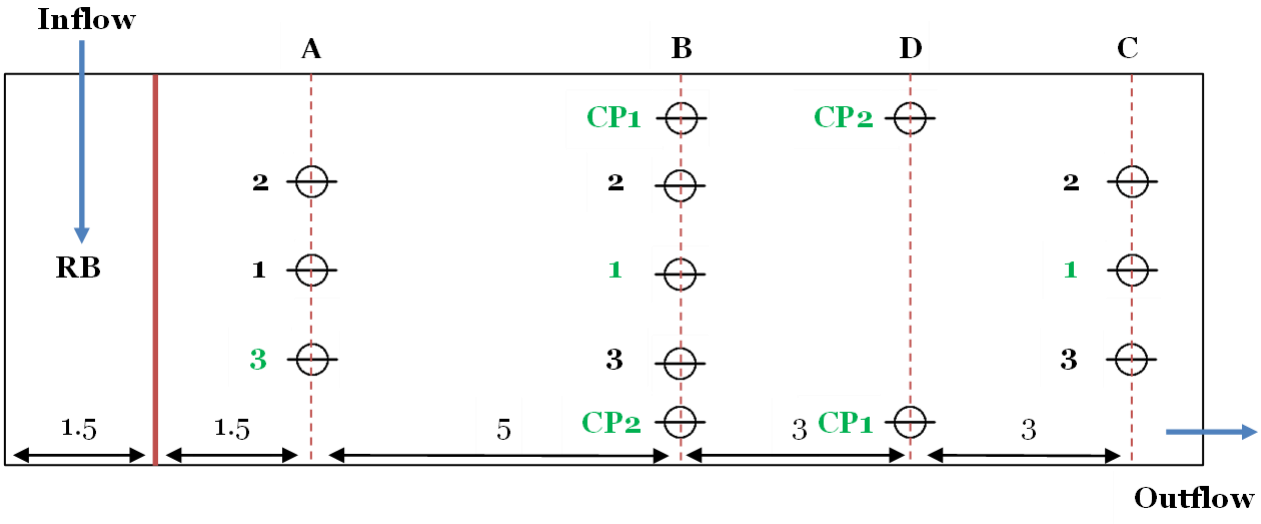

Figure 6. Plan view of the artificial aquifer system, Tank 1. The piezometres used as pumping and/or observation wells are highlighted in green, and all values are expressed in units of metres.

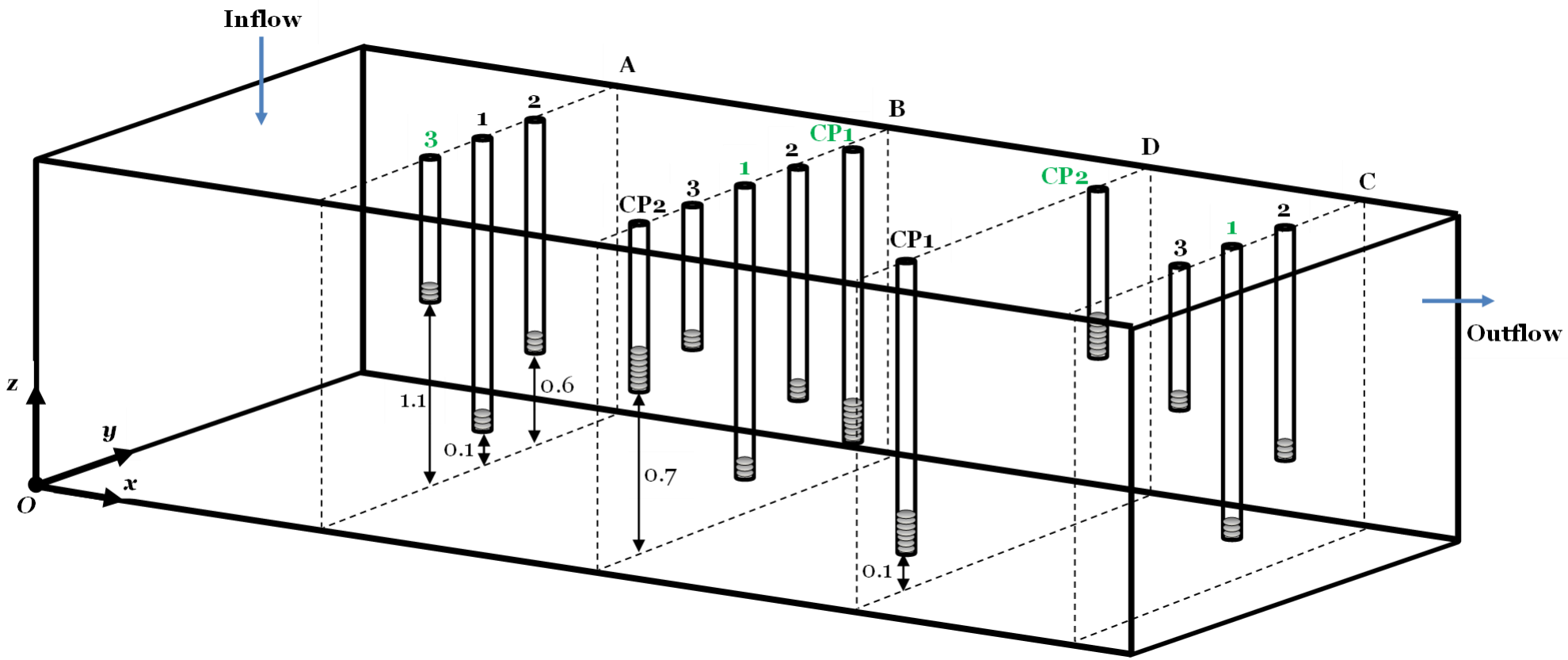

Figure 7. Oblique projection of the artificial aquifer system, Tank 1. The piezometres used as pumping and/or observation wells are highlighted in green, and all values are expressed in units of metres.

2.2 Hydraulic tests: pumping & recovery

A total of four pumping tests were carried out on Tank 1 between the 23rd and the 28th of March of 2022. Each test was performed in a different piezometre, which were: **B1**, **BCP1**, **A3**, and **DCP2**. The duration of pumping was 3 h in all cases except for piezometre A3, which ran dry after 0.5 h, thus forcibly ending the test. Following each pumping test, the artificial aquifer was allowed to recover for at least 20 h to ensure the hydraulic heads returned to the initial level.

The monitoring of the hydraulic head began 12 days before the execution of the first test with a measurement frequency of 30 min, in order to identify any regional tendencies in the hydraulic level. For the pumping tests, the measurement frequency was changed to 5 s.

During the recovery periods, the hydraulic heads continued to be monitored, and with the same frequency of measurement. For the pumping test performed on DCP2, the recovery period was cut short, to approximately 5 h, due to an infiltration of water from Tank 2 which created an uncontrolled external perturbation to the system. The rate of recharge of water into the system and flow rate of pumping were approximately 1.0 and 0.7 L min^{-1}, respectively. This information is summarised in Table 1 below.

Table 1. Summary of hydraulic test parameters.

Pumping test	Piezometre	Duration of pumping / h	Rate of recharge / L min^{-1}	Rate of extraction / L min^{-1}
1	B1	3.0		
2	BCP1	3.0		
3	A3	0.5	≈ 1.0	≈ 0.7
4	DCP2	3.0		

Immediately prior to each pumping test, the groundwater levels in the nine piezometres distributed across the tank were measured manually using a water-level metre. These groundwater levels were taken in terms of depth to water table (d_{wt} in Figure 8, below). The water-level metre was also used during the pumping tests, with measurements taken periodically to observe the change throughout.

The hydraulic head was monitored using TD-divers (Schlumberger water services, Delft, The Netherlands) hung from strings attached to the top of each piezometre. Divers are data-logging devices which measure the total pressure exerted on them from above, expressed in terms of length (*e.g.*, centimetres). For a submerged diver, this includes the pressure exerted by the water column above the diver and the pressure exerted by the atmosphere ($h_{\text{TD-diver}}$). In order to obtain the pressure due to the water column only, a barometric pressure diver was used to measure the atmospheric pressure (h_{baro}). The values from the latter are matched to those of the TD-diver with the same timestamp and then subtracted from it:

$$h_{\text{wc}}(t) = h_{\text{TD-diver}}(t) - h_{\text{baro}}(t) \tag{4}$$

The barometric diver is placed at the discharge point of the tank, at the same height at which is set the discharge pipe.

The water-level metre and diver readings are not directly comparable, with one measuring groundwater level as depth to water table from the surface of the ground, and the other measuring the height of the water column. Nevertheless, the manual water-level metre readings provide a simple method of verifying the diver readings.

The readings from the divers are converted into a format in which the hydraulic head is expressed with respect to the bottom-left corner of the tank (point *O*, as shown in the oblique projection in Figure 7 above, and in the diagram in Figure 8 below). This creates a uniform reference system that allows all hydraulic heads to be directly comparable. For a given piezometre, i, whose top edge is at a known height above the reference point, $h_{i,\text{pz}}$, the length of the string from which the diver hangs, l_i, is subtracted and the water column height, $h_{i,\text{wc}}$, is added:

$$h_{i,\text{O}} = h_{i,\text{pz}} - l_i + h_{i,\text{wc}} \tag{5}$$

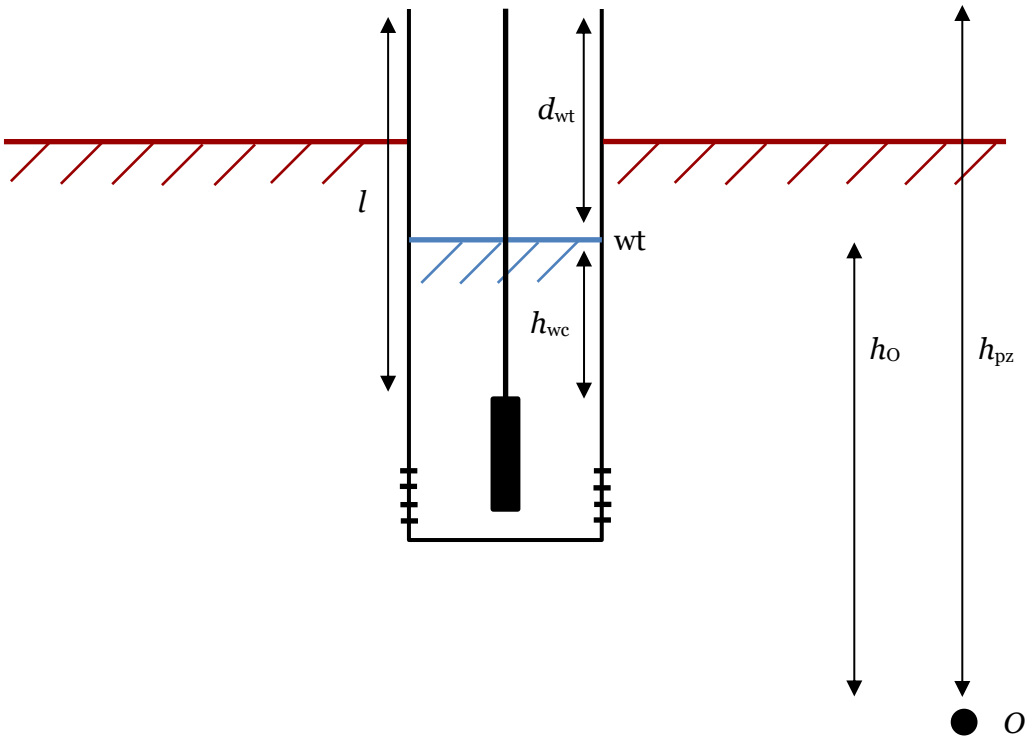

Figure 8. Diagram of piezometre setup with TD-diver, where wt is the water table, d_{wt} is the depth to water table measured using the manual metre, h_{wc} represents the height of the water column (calculated as the difference between the readings of the TD-diver and the barometric diver, $h_{TD\text{-}diver} - h_{baro}$), l is the length of string from which the diver is hung, h_{pz} is the height of the top edge of the piezometre with respect to the origin, O, one of the bottom corners of Tank 1, and h_O is the hydraulic head relative to the origin, O.

2.3 Dissolved oxygen monitoring

A series of dissolved oxygen (DO) sensors were placed in close proximity to the four piezometres which served as pumping wells in order to monitor any changes in levels brought about by the pumping tests. Five sensors were placed in each location (constant x, y), each at a different depth (variable z), as shown in Figure 9.

The DO concentration was monitored with a measurement frequency of 5 s, using two OXY-10 SMA oxygen metres and twenty PSt3 type oxygen dipping probes as sensors, both purchased from PreSens Precision Sensing GmbH (Regensburg, Germany). The sensor is a polymer optical fibre with one end coated in an oxygen-sensitive foil and has a detection limit of 15 ppb (0.015 ppm). In addition, five temperature sensors (Pt100 model) from the same manufacturer were used to account for temperature fluctuations. A Savitzky-Golay smoothing filter was applied to each oxygen concentration dataset using a window length of 51 and fitted using a second-order polynomial.

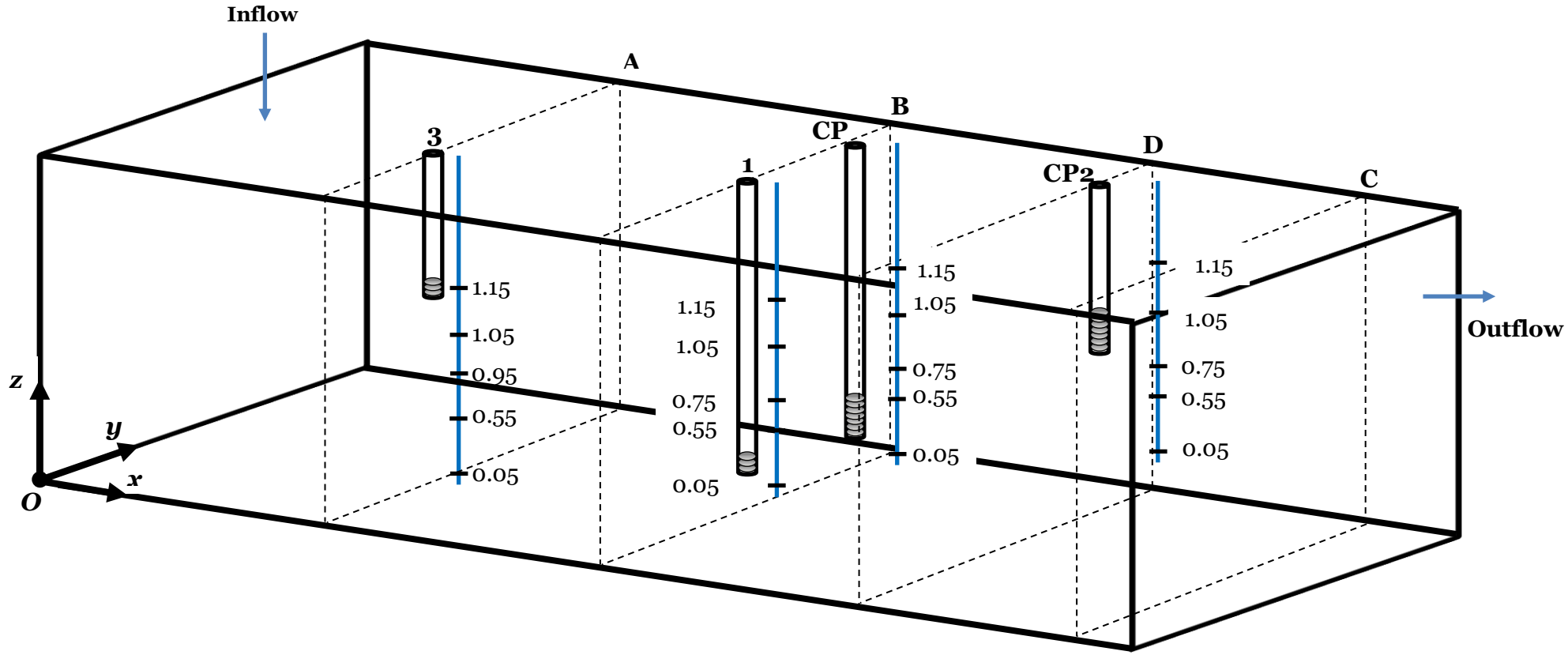

Figure 9. Oblique projection of the artificial aquifer system, Tank 1, with the placement of the dissolved oxygen sensors shown. The values represent the heights of the sensors with respect to the base of the tank, and are expressed in units of metres.

2.4 Interpretation of the hydraulic tests

The procedure of a pumping test consists in creating a controlled hydraulic perturbation by either extracting or injecting water, typically at a constant flow rate, out of a single piezometre and observing the change in hydraulic head in various points in the surrounding area. In the present study, only extraction of groundwater was performed.

The extraction causes a drawdown in the hydraulic head. This drawdown, s, is defined as the difference between the initial hydraulic head, $h(t_0)$, prior to perturbation and the hydraulic head at time t, $h(t)$. Once pumping is stopped, the hydraulic head stops decreasing and starts to recover the hydraulic head, until eventually drawdown is 0.

$$s(t) = h(t_0) - h(t) \tag{6}$$

There are various methods for interpreting the drawdown and recovery produced by the pumping test. The most common ones were designed with the same set of assumptions:

- The aquifer is confined, homogeneous, has uniform thickness, and infinite extent
- The water table was horizontal prior to pumping
- The pumping rate is constant
- The well is fully penetrating
- The piezometre diameter is small enough that well-storage is negligible
- The flow towards the pumping piezometre is radial (two-dimensional)

One may find these assumptions to be quite limiting, and particularly inappropriate for the present study given the heterogeneous and unconfined nature of the aquifer in question. However, it has been shown that most of these methods are valid even for aquifers that do not fulfil all of the criteria set out, as will be discussed further in this section.

2.4.1 Theis drawdown method

The classical analysis for hydraulic pumping tests is the Theis solution (1935). Given the conditions listed above, Theis expressed the analysis with the following governing equation:

$$\nabla^2 h = \frac{S}{Kb}\frac{\partial h}{\partial t} \tag{7}$$

Where ∇^2 is the Laplacian operator (the sum of the second partial derivatives of the function in the x, y, and z dimensions):

$$\nabla^2 = \frac{\partial^2}{\partial x^2} + \frac{\partial^2}{\partial y^2} + \frac{\partial^2}{\partial z^2} \tag{8}$$

h is hydraulic head, S is storativity, K is hydraulic conductivity, b is saturated aquifer thickness, and $\frac{\partial h}{\partial t}$ is the change in hydraulic head as a function of time. The boundary condition at the piezometre ($r = r_{pz}$), corresponding to the lower boundary, is:

$$q = \frac{Q_{pz}}{2\pi r b} \tag{9}$$

where q is the flux at the piezometre, Q_{pz} is the pumping rate at the piezometre, and r is the radius of the piezometre. The boundary condition at $r = \infty$ (since the aquifer is assumed to be infinite), corresponding to the upper boundary, is:

$$h = h_o \tag{10}$$

which implies that the hydraulic head is equal to the initial hydraulic head, prior to the perturbation created by pumping. In other words, the effect from the pumping is localised around the point at which it is occurring, the hydraulic head at the outer boundary of the aquifer is not affected by it.

Theis thus devised the following analytical solution to the problem:

$$s = \frac{Q}{4\pi K b} \int_u^\infty \frac{e^{-x}}{x} dx \tag{11}$$

where e is Euler's number (2.718…), and u is a dimensionless parameter, $u = \frac{r^2 S}{4Tt}$.

The exponential integral can be represented by $W(u)$ (termed the well function), and the product of Kb as transmissivity, thus simplifying to the following expression:

$$s(r,t) = \frac{Q}{4\pi T} W(u) \tag{12}$$

Since the rest of the components are known, and even fixed in the cases of Q and r, the Theis well function can be solved for different values of T and S until the best fit to the observed data is obtained.

Nowadays, the computing power available makes this task relatively straightforward, however, at the time when this solution was devised, the calculations and subsequent plotting had to be done by hand, which was a tedious task. To overcome this, Cooper and Jacob (1946) devised an approximation for late times or small radial distances from the pumping well.

2.4.2 Cooper-Jacob approximation

The exponential integral can be expressed as an infinite Taylor series:

$$W(u) = -\gamma - \ln(u) + u + \frac{u^2}{2 \cdot 2!} + \frac{u^3}{3 \cdot 3!} + \ldots \tag{13}$$

Where γ is the Euler constant (0.5772...). Remembering that u is inversely proportional to time, it is clear that as t becomes larger, u will become smaller, which is compounded by the increasing indices in the series expansion (e.g., $0.1^2 > 0.1^3$). Similarly, since u is directly proportional to r, for short radial distances between the pumping well and the observation well, u will be negligibly small.

This implies that for the late time data (where t is largest), u will be negligible, and hence the expansion can be truncated:

$$W(u) \approx -\gamma - \ln(u) \tag{14}$$

$$W(u) \approx -\ln(1.78) - \ln(u) = \ln\left(\frac{1}{1.78u}\right) \tag{15}$$

$$W(u) \approx \ln\left(\frac{4Tt}{1.78r^2S}\right) \tag{16}$$

This can be plugged into the drawdown function:

$$S(r,t) = \frac{Q}{4\pi T} \ln\left(\frac{4Tt}{1.78r^2S}\right) \tag{17}$$

To follow convention, the logarithm is transformed to base 10:

$$\ln(x) = \ln(10) \log_{10}(x) \tag{18}$$

$$\ln(x) = 2.303 \log_{10}(x) \tag{19}$$

$$s(r,t) = \frac{2.3Q}{4\pi T} \log\left(\frac{4Tt}{1.78r^2S}\right) \tag{20}$$

Thus, the Theis well function simplifies to a linear equation which can be evaluated to give the transmissivity (based on the gradient) and the storativity (based on the x-intercept, which is the point of zero drawdown, t_o, and transmissivity):

$$s(r,t) = \frac{2.3Q}{4\pi T} \log(t) + \log\left(\frac{2.25T}{r^2 S}\right) \tag{21}$$

$$y = m \cdot x + c$$

It must be highlighted that for this approximation to be valid, the authors stated that the value of u for the selected data points must be less than 0.02, *i.e.*, for late-times or short radial distances between pumping piezometre and observation piezometre. However, more recently the consensus has arrived at $u < 0.03$, which produces an approximation error of 1% with respect to the full Theis equation (Meier *et al.*, 1998).

2.4.3 Theis recovery method

Once pumping has ended, the hydraulic head gradually recovers to its natural level. This will ideally be identical to the head prior to the induced perturbation, but in some cases may be altered due to natural perturbations, such as rainfall, which must be taken into account in the analysis. The rate of change of hydraulic head during recovery can also be used to estimate the hydraulic parameters of the aquifer. Several solutions have been devised over the years, each with advantages and disadvantages.

Traditionally, this has been done with the Theis recovery method (1935), in which the residual drawdowns (data points after the end of pumping and before full recovery) are plotted against the base 10 logarithm of $\frac{t - t_i}{t - t_f}$, where t is time, t_i is the time at which pumping started, and t_f is the time at which pumping finished.

Conceptually, the recovery can be considered as follows: the pumping from the well continues with a constant flow rate Q, but starting from $t = t_f$ there is an equivalent recharge of water with flow rate Q, as illustrated in Figure 10 below. In other words, the two flow rates are superimposed to give the final solution.

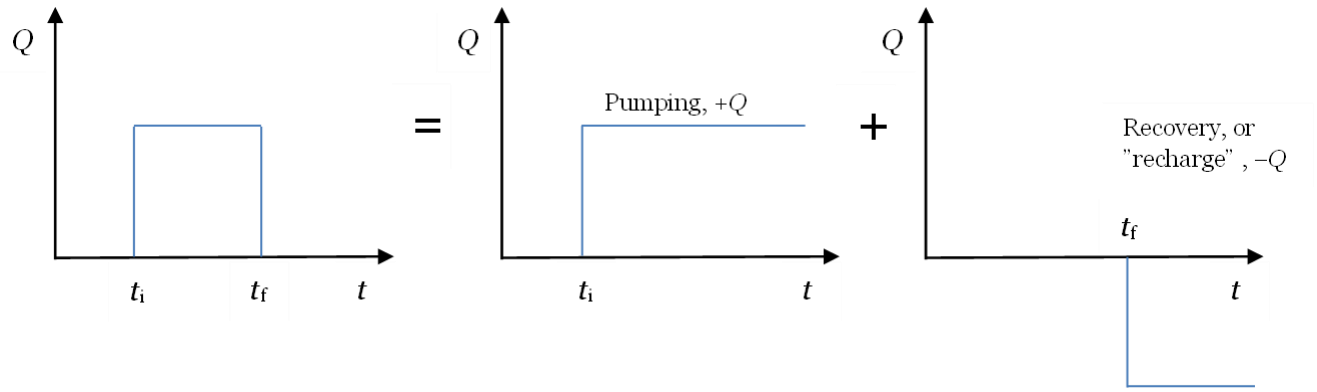

Figure 10. Diagram to illustrate the concept behind the Theis recovery method (adapted from Sánchez-Vila and Batista, 2009).

For a confined aquifer in a transient state and at late times, the residual drawdown can be expressed as:

$$s(t) = \frac{Q}{4\pi T} \ln\left(\frac{2.25T(t - t_i)}{r^2 S}\right) - \frac{Q}{4\pi T} \ln\left(\frac{2.25T(t - t_f)}{r^2 S}\right) \quad (22)$$

As most of the terms in the logarithm cancel out, and once again converting the natural logarithm to base 10, the function becomes:

$$s(t) = \frac{2.3Q}{4\pi T} \log\left(\frac{t - t_i}{t - t_f}\right) \quad (23)$$

which plots as a straight line that passes through the origin ($c = 0$), with a gradient from which the transmissivity can be estimated. Clearly, however, it does not provide an estimate for the storativity coefficient.

2.4.4 Agarwal recovery method

Various other methods have been devised to overcome this shortcoming, but the most popular is the one conceived by Agarwal (1980), which treats the recovery data as if it were drawdown resulting from pumping.

Just like Theis before him, Agarwal designed this method for confined, homogeneous, and ideally large aquifers, which undergo pumping at a constant rate for a sufficiently long time. When these conditions are met, flow toward the pumping well is radial and the Cooper-Jacob approximation holds true. Thus, based on the same superposition principle described in the Theis recovery method, Agarwal 'drawdown' is defined as:

$$s_A(t) = s(t_f) - s_R(t) = s(t_f) - (s(t) - s(t - t_f)) \quad (24)$$

where $s(t_f)$ is the drawdown at the time when pumping is stopped (t_f), $s_R(t)$ is the residual drawdown at $t > t_f$, and $s(t)$ is the drawdown at an arbitrary time t. The Agarwal drawdown can also be expressed as:

$$s_A(t) = \frac{Q}{4\pi T}\left[\ln\left(\frac{2.25Tt_f}{r^2S}\right) - \ln\left(\frac{2.25Tt}{r^2S}\right) - \ln\left(\frac{2.25T(t-t_f)}{r^2S}\right)\right] \quad (25)$$

$$= \frac{2.3Q}{4\pi T}\log\left(\frac{2.25Tt_A}{r^2S}\right) \quad (26)$$

Where the Agarwal time, t_A, is implicitly defined as $t_A = t_f \cdot (t - t_f) / t$. Trabucchi *et al.* (2018) have shown that this method works well in "nearly all" aquifer conditions, delivering reliable hydraulic parameter estimates as long as the pumping rate is constant, and the characteristic time, $t_c\left(\frac{r^2S}{T}\right)$, at the piezometre is small. In practical applications, the latter condition is almost always fulfilled at the pumping piezometre, where the radius used is that of the piezometre, but this is not the case for observation piezometres, where the radius (distance between pumping and observation piezometres) can be many tens of metres. They also found that this method worked very well for late recovery times, but was less than ideal at early times, *i.e.*, the time immediately after pumping has stopped, which entails losing valuable data. It also implies that the method requires the pumping time to be sufficiently long; they found that if radial flow is not achieved because of too short a pumping time (which can be identified by a constant gradient in the semi-log Cooper-Jacob plot), the pumping drawdown curves are not reproduced correctly. The minimum pumping time they suggest is $10t_c$.

In view of this, Trabucchi *et al.* proposed modifications to the Agarwal method that addresses the shortcomings of the original.

2.4.5 Modified Agarwal recovery method

Once again, the residual drawdown is used to produce a

$$s_M(t - t_f) = s_{ap}(t) - s_R(t) \quad (27)$$

Where t includes only the time after recovery has started ($t > t_f$), s_M is the modified Agarwal drawdown, s_R is the residual drawdown, and s_{ap} is an approximation of drawdown whose definition depends on whether the system is two-dimensional (radial flow) or higher. For the present study, only radial flow was assumed, which defines s_{ap} as:

$$s_{ap}(t) = s(t_f)\frac{m}{2.3}\log_{10}\frac{t}{t_f} \quad (28)$$

Where m is the gradient of the drawdown data on a semi-log plot.

In this study, the drawdowns were analysed using the Cooper-Jacob approximation, and the recoveries were analysed with the Theis, Agarwal, and modified Agarwal methods.

3. Results & discussion

3.1 Hydraulic tomography

The hydraulic head at each piezometre is plotted against time in Figure 11, each plot corresponding to a single pumping test. The times are expressed relative to the start of pumping for each test, which is defined as t = 0. The plots show how the drawdown always began sharply at t = 0, indicating little to no delay in aquifer response to pumping, which demonstrates negligible well-storage. Both the drawdowns and the recoveries were generally smooth, and the initial hydraulic head was clearly recovered after each test, thus one can conclude that no external perturbations affected the system.

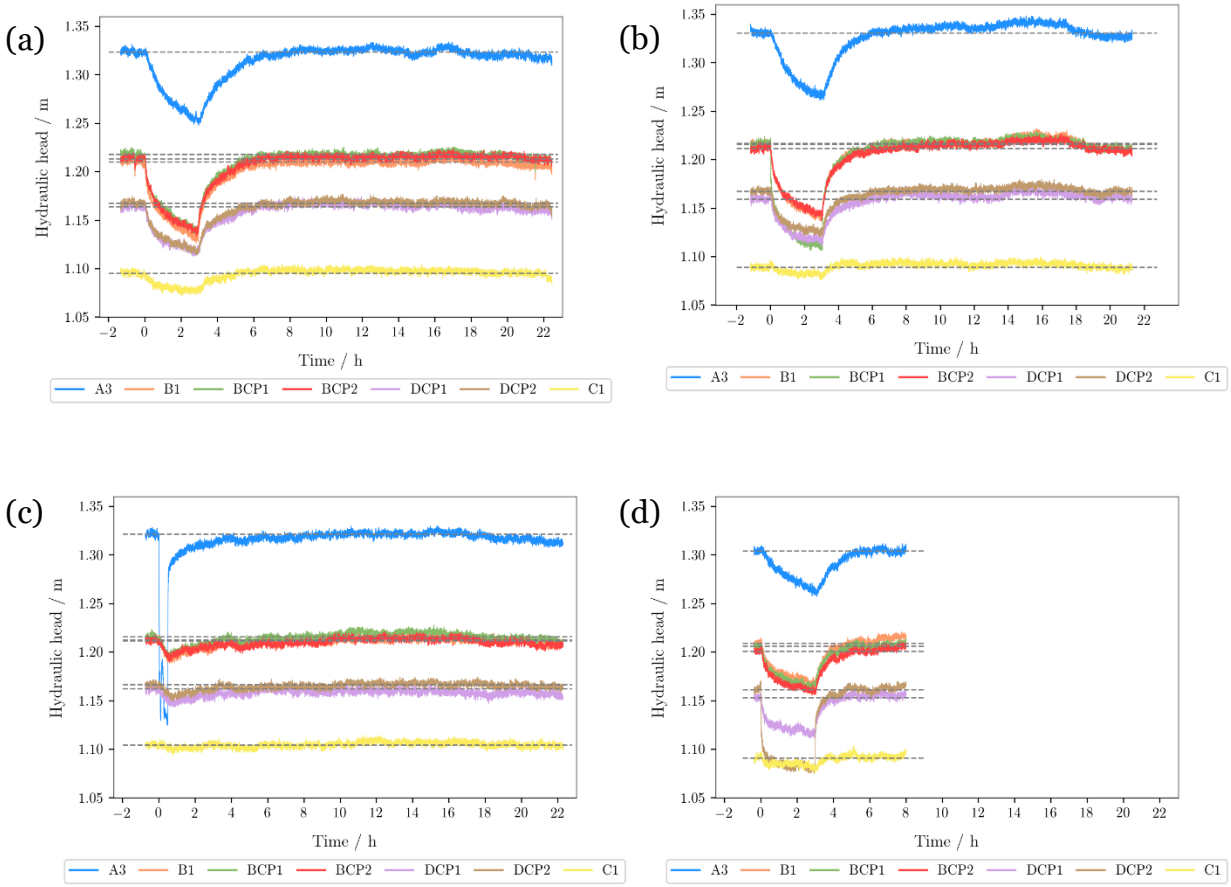

Figure 11. Hydraulic heads for the four pumping tests a) extraction from piezometre B1; b) extraction from piezometre BCP1; c) extraction from piezometre A3; d) extraction from piezometre DCP2.

The only exception to the statement regarding smooth drawdown was piezometre A3 on PT3 (Figure 11(c)), which ran dry shortly after pumping began there, causing the sensor to produce an irregular signal. That this occurred only in this piezometre is explained by the fact that it is the shallowest well to be pumped from (1.1 m from the base of the tank, 0.30 m from ground surface). Once pumping was halted, the recoveries were fairly regular, however, the brevity of the pumping period meant that the drawdown in the rest of the piezometres was very slight, even absent in the case of C1 (which also happens to be furthest away from A3), with the implication that the data for this pumping test is not of the same quality as the rest.

Similarly, an issue with the recharge pump in the adjoining tank during the recovery period of pumping test 4 caused an overflow of water into the system under study. This resulted in the hydraulic head to increase substantially, far beyond the initial level. Hence, the hydraulic head data for this test had to be truncated to the point immediately prior to the external perturbation starting, $t = 8$ h. This means that the recovery period is slightly shorter than recommended by hydrogeological convention (at least three times the duration of pumping), therefore there is lower confidence in the validity of this recovery data and any interpretation derived from it. The drawdown data, nonetheless, appears normal and should produce an acceptable result.

The piezometres in sections A, B, and D showed noticeable responses in all pumping tests, including in the short third test. Piezometre C1, on the other hand, consistently produced the smallest response. The most significant drawdown at this piezometre following a full pumping test occurred during PT1 (pumping from B1) with a 2.4 cm decrease in hydraulic head, and just over 1 cm decreases for PT2 (pumping from BCP1) and PT4 (pumping from DCP2). Its lower response to pumping in DCP2 and BCP1 compared to B1, despite being physically closer to DCP2 than to B1, is an early indication of the presence of a less permeable section acting as a barrier to flow between the centre of the aquifer and the BCP1-DCP2-C2 corridor. Unfortunately, the lack of well-defined drawdown and recovery at C1 for any of the pumping tests suggests the data will not lend itself as well to a regression analysis and precludes more detailed analysis.

The three piezometres in section B have consistently similar values of hydraulic head (both initial and minimum) and reach minimum hydraulic head (*i.e.*, maximum drawdown) at approximately the same time (see Table 2). This suggests that this section of aquifer is fairly uniform in hydraulic terms, although the connectivity between them is left to be determined.

Simply through visual observation of the plots, one can perceive that the drawdowns begin with a very sharp, high gradient but rapidly lower to a more moderate one, corresponding to a transient regime. The hydraulic heads then approach a steady state (*i.e.*, the gradient tends

to 0) in most observation points, while pumping is still active. This can also be seen via a brief comparison of the time at which minimum hydraulic head ($t(h_{min})$) is reached at each point (Table 2) and the time at which pumping ended (t_f) (Table 3). For PT1, all points except A3 reached h_{min} several minutes before pumping was stopped; for PT2, the difference was not so stark, but $t(h_{min})$ was smaller than t_f in all points, including A3; and PT4 followed the same pattern as PT1. PT3 was, as usual, the only exception ($t_f < t(h_{min})$ in all cases), which is easily explained by the exceedingly short pumping period not allowing the system to approach a steady state.

Table 2. Summary of some characteristic hydraulic head parameters at key points in time.

Piezometre	Initial hydraulic head, $h(t_o)$ / m				Minimum hydraulic head, h_{min} / m				Time of minimum hydraulic head, $t(h_{min})$ / min			
	PT1	PT2	PT3	PT4	PT1	PT2	PT3	PT4	PT1	PT2	PT3	PT4
A3	1.324	1.331	1.322	1.304	1.248	1.261	1.125	1.257	178.0	174.3	—	185.2
B1	1.210	1.216	1.213	1.209	1.126	1.137	1.189	1.164	169.6	177.3	34.4	159.3
BCP1	1.218	1.217	1.216	1.206	1.134	1.106	1.192	1.160	169.6	176.7	34.9	168.2
BCP2	1.214	1.212	1.212	1.201	1.133	1.137	1.190	1.156	170.4	180.1	35.6	169.3
DCP1	1.164	1.160	1.162	1.153	1.113	1.110	1.144	1.111	161.4	181.2	38.1	164.0
DCP2	1.168	1.168	1.167	1.162	1.114	1.120	1.150	1.075	169.6	175.3	38.3	176.2
C1	1.095	1.089	1.105	1.091	1.071	1.076	1.093	1.076	122.4	177.1	46.9	178.4

Table 3. Summary of pumping duration for each test.

Pumping test	Pumping duration / min
1	176
2	183
3	29
4	180

Figure 12 shows a representation, not to scale, of the hydraulic gradient in the aquifer before being subjected to pumping. This was done using the average hydraulic head measured in sections A and C prior to the tests, and produces a gradient of approximately 0.020 m m^{-1}:

$$\frac{\Delta h}{\Delta l} = \frac{1.325 - 1.10}{14 - 3} \tag{29}$$

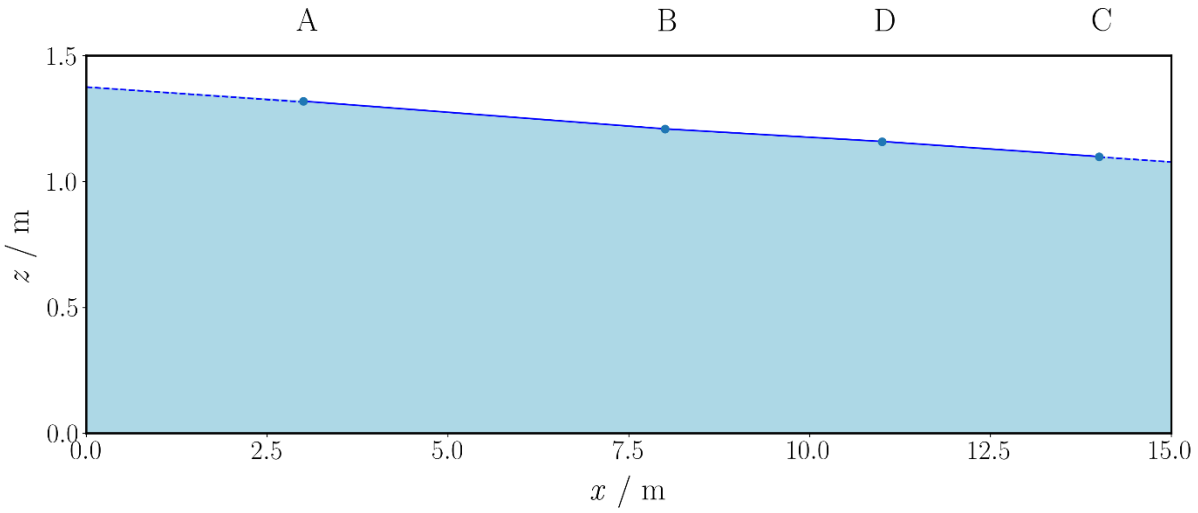

Figure 12. Representation of the hydraulic gradient in the aquifer prior to hydraulic perturbation via pumping. Not to scale.

Given the hydraulic gradient and the scale of the aquifer, the aquifer thickness can be considered uniform. Additionally, the hydraulic head in the mid-point of the tank (x = 7.5 m) can be interpolated (1.227 m) and used as the average value to calculate the aquifer hydraulic conductivity, K.

The hydraulic head data for each piezometre and across the four pumping tests were transformed into drawdown ($s(t) = h(t) - h(t_0)$) and analysed using the four methods described in section 2.5. Figure 13 shows the collection of plots produced for piezometre A3 for the first pumping test. They are organised in rows by method, from top to bottom: drawdown via the Theis solution, recovery via the Theis solution, recovery via the Agarwal solution, and recovery via the modified Agarwal solution. The plots in the left column express time on a linear scale, and those in the right column are semi-log plots with time on a $\log_{10}$ scale. The latter were used to perform the regression analysis on the linear, late-time portions of the plots (*i.e.*, where the Cooper-Jacob approximation is valid) and obtain estimates of effective transmissivity and estimated storativity. The plots for the rest of the piezometres and pumping tests can be found in the Appendix.

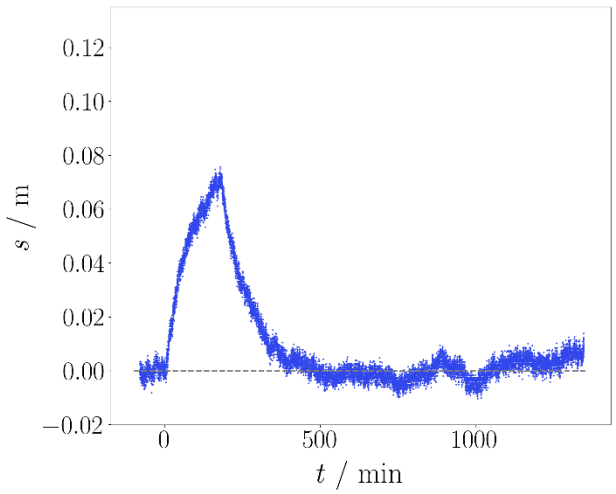
0.12
0.10
0.08
0.06
0.04
0.02
0.00
−0.02
s / m
0
500
1000
t / min

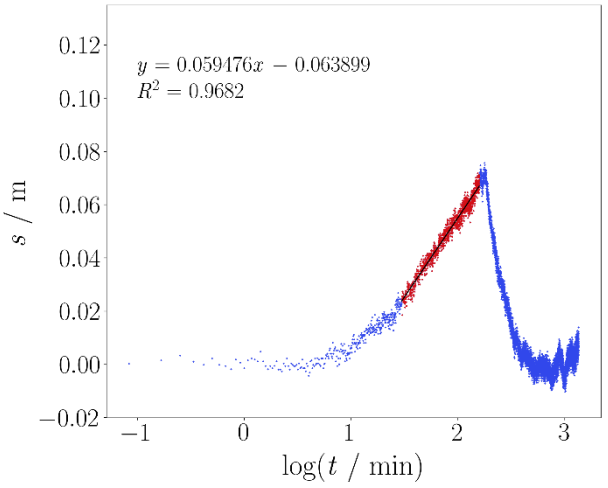
y = 0.059476x − 0.063899
R² = 0.9682
0.12
0.10
0.08
0.06
0.04
0.02
0.00
−0.02
s / m
−1
0
1
2
3
log(t / min)

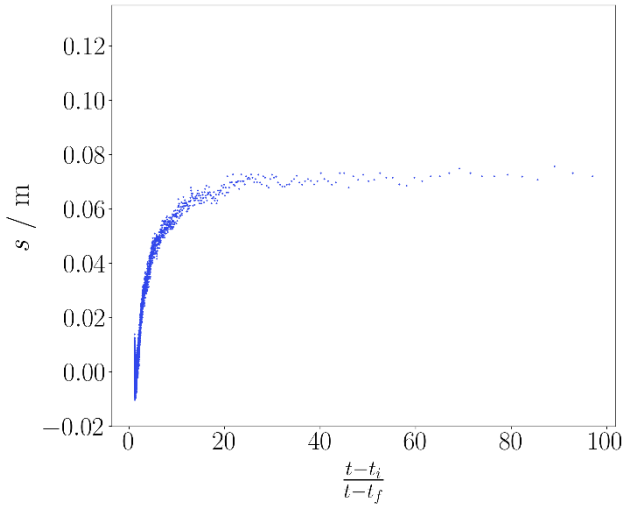
0.12
0.10
0.08
0.06
0.04
0.02
0.00
−0.02
s / m
0
20
40
60
80
100
(t−t_i)/(t−t_f)

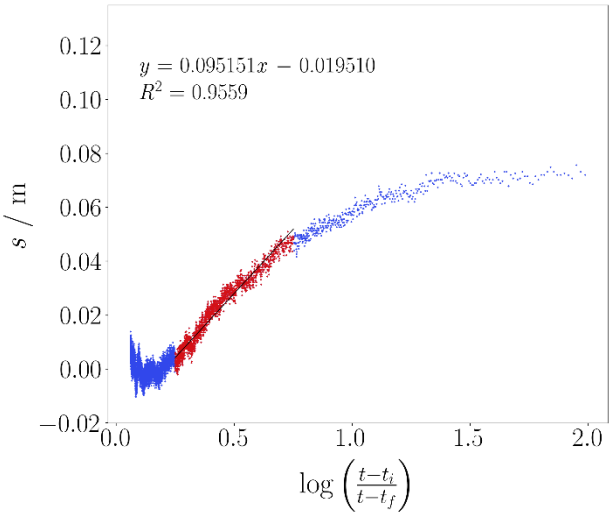
y = 0.095151x − 0.019510
R² = 0.9559
0.12
0.10
0.08
0.06
0.04
0.02
0.00
−0.02
s / m
0.0
0.5
1.0
1.5
2.0
log((t−t_i)/(t−t_f))

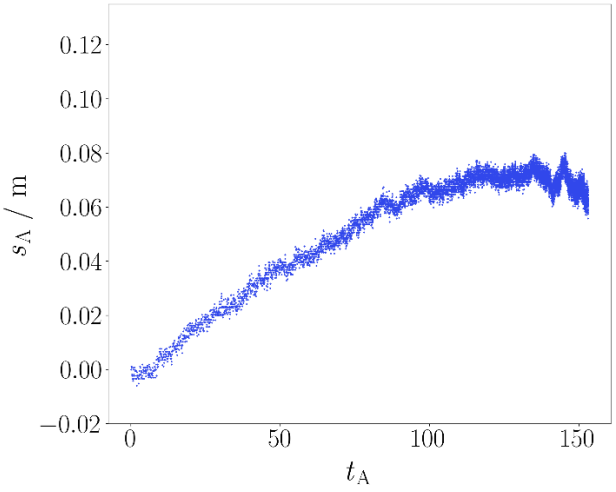
0.12
0.10
0.08
0.06
0.04
0.02
0.00
−0.02
s_A / m
0
50
100
150
t_A

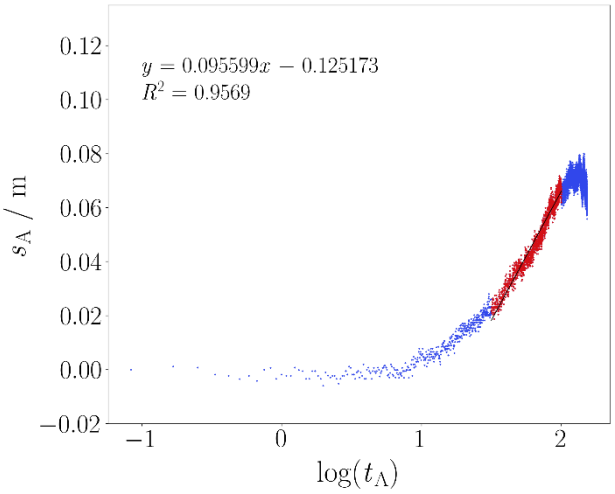
y = 0.095599x − 0.125173
R² = 0.9569
0.12
0.10
0.08
0.06
0.04
0.02
0.00
−0.02
s_A / m
−1
0
1
2
log(t_A)

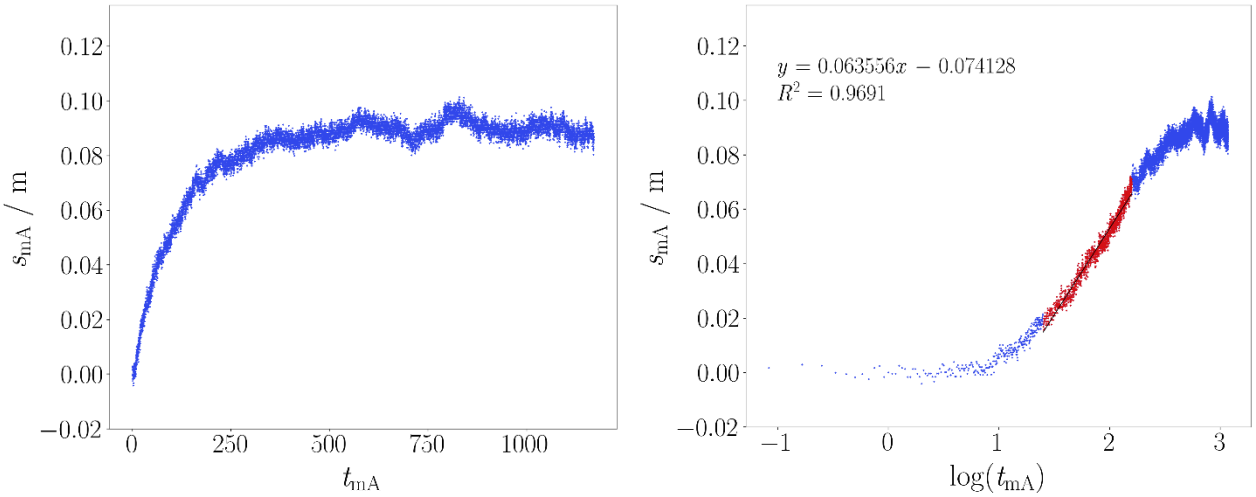

Figure 13. Linear regression analyses of drawdown and recovery data for piezometre A3 for PT1. The plots in the left column have time on a linear scale, and those in the right column have time on a $\log_{10}$ scale. The plots are organised in rows by method, from top to bottom these are: Theis drawdown, Theis recovery, Agarwal recovery, and modified Agarwal recovery.

In order to verify that the selected data points comply with the CJ approximation, the parameter u was calculated for the drawdown analysis of each pumping test and plotted against $\log(t)$. Figure 14 shows the range of values u takes at each piezometre for the drawdown analysis of PT1, from which it can be clearly observed that none of the points come close to exceeding the accepted maximum established as u = 0.03, demonstrating the suitability of the selected range of datapoints. The equivalent plots for the other pumping tests can be found in the Appendix (figures A.14, A.22. and A.30).

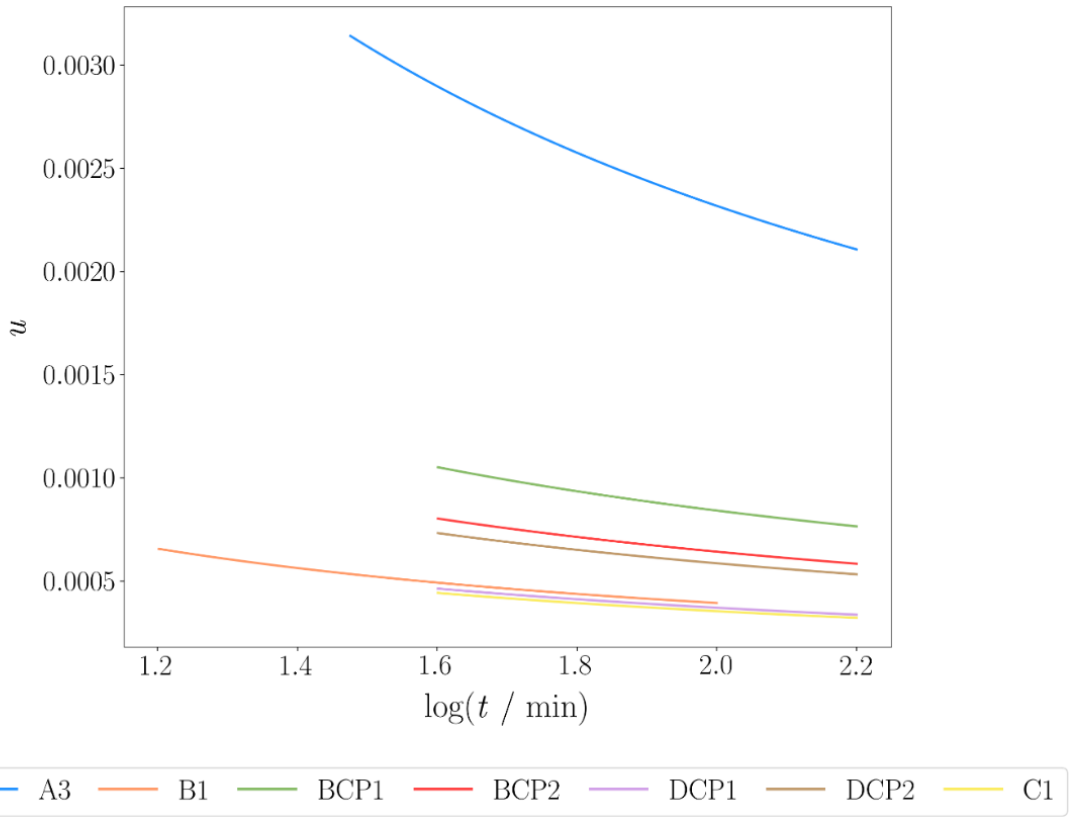

Figure 14. Plot of u versus log(t) for the data used in the drawdown analysis of pumping test 1, to demonstrate the validity of the range of datapoints selected.

The hydraulic parameters calculated based on the linear regressions are summarised in tables 4 to 10. Each table corresponds to a single piezometre and includes the values for all the pumping tests and the four analytical methods employed.

Table 4. Hydraulic parameters determined for piezometre A3.

Pumping test	Theis draw-down	Theis recovery	Agarwal re-covery	Modified Agarwal recovery	Geometric average	GSDF§
	Effective transmissivity, T_{eff} / m² d⁻¹					
PT1	3.1	1.9	1.9	2.9	2.4	1.25
PT2	3.1	2.5	2.4	3.0	2.8	1.12
PT3*	—	2.8	2.1	—	—	—
PT4	5.4	3.2	3.2	4.2	3.9	1.24
	Hydraulic conductivity, K / m d⁻¹					
PT1	2.5	1.6	1.6	2.4	—	—
PT2	2.6	2.0	2.0	2.5	—	—
PT3*	—	2.2	1.7	—	—	—
PT4	4.4	2.6	2.6	3.5	—	—
	Estimated storativity, S_{est}					
PT1	2.30×10^{-3}	—	2.46×10^{-3}	2.66×10^{-3}	2.47×10^{-3}	1.04
PT2	2.44×10^{-3}	—	2.07×10^{-3}	2.50×10^{-3}	2.33×10^{-3}	1.03
PT3	—	—	—	—	—	—
PT4	1.86×10^{-3}	—	1.29×10^{-3}	1.40×10^{-3}	1.50×10^{-3}	1.13

* Low confidence. § Geometric standard deviation factor.

Table 5. Hydraulic parameters determined for piezometre B1.

Pumping test	Theis drawdown	Theis recovery	Agarwal recovery	Modified Agarwal recovery	Geometric average	GSDF§
	Effective transmissivity, T_{eff} / m² d⁻¹					
PT1	4.9	3.7	3.9	4.4	4.2	1.11
PT2	4.8	3.4	3.9	4.3	4.1	1.13
PT3*	6.5	4.2	2.8	9.9	5.2	1.60
PT4	9.3	5.0	5.4	6.2	6.3	1.27
	Hydraulic conductivity, K / m d⁻¹					
PT1	4.0	3.0	3.2	3.6	—	—
PT2	3.9	2.8	3.2	3.5	—	—
PT3*	5.3	3.5	2.3	8.1	—	—
PT4	7.6	4.1	4.4	5.1	—	—
	Estimated storativity, S_{est}					
PT1	—	—	—	—	—	—
PT2	3.35×10^{-2}	—	4.33×10^{-2}	3.97×10^{-2}	3.86×10^{-2}	1.09
PT3*	2.61×10^{-3}	—	3.23×10^{-3}	1.21×10^{-2}	4.67×10^{-3}	1.48
PT4	2.78×10^{-3}	—	5.14×10^{-3}	5.32×10^{-3}	4.24×10^{-3}	1.28

* Low confidence. § Geometric standard deviation factor.

Table 6. Hydraulic parameters determined for piezometre BCP1.

Pumping test	Theis draw-down	Theis re-covery	Agarwal recovery	Modified Agarwal re-covery	Geometric average	GSDF§
	Effective transmissivity, T_{eff} / m² d⁻¹					
PT1	3.8	3.7	2.9	4.3	3.6	1.16
PT2	4.6	3.5	3.8	4.5	4.1	1.11
PT3*	6.5	5.6	2.5	11.5	5.7	1.73
PT4	8.7	4.6	5.8	7.4	6.5	1.27
U	Hydraulic conductivity, K / m d⁻¹					
PT1	3.1	3.0	2.3	3.5	—	—
PT2	3.7	2.9	3.074	3.6	—	—
PT3*	5.3	4.5	2.0	9.4	—	—
PT4	7.1	3.7	4.8	6.0	—	—
	Estimated storativity, S_{est}					
PT1	5.42×10^{-2}	—	6.02×10^{-2}	4.26×10^{-2}	5.18×10^{-2}	1.03
PT2	—	—	—	—	—	—
PT3*	2.51×10^{-3}	—	2.71×10^{-3}	5.92×10^{-3}	3.42×10^{-3}	1.22
PT4	3.03×10^{-3}	—	5.19×10^{-3}	5.75×10^{-3}	4.49×10	1.26

* Low confidence. § Geometric standard deviation factor.

Table 7. Hydraulic parameters determined for piezometre BCP2.

Pumping test	Theis draw-down	Theis re-covery	Agarwal recovery	Modified Agarwal re-covery	Geometric average	GSDF§
	Effective transmissivity, T_{eff} / m² d⁻¹					
PT1	4.3	4.1	3.2	4.6	4.0	1.14
PT2	5.1	4.0	4.1	4.8	4.5	1.11
PT3*	7.4	7.7	3.5	12.7	7.1	1.58
PT4	7.6	4.4	5.5	6.9	6.0	1.24
	Hydraulic conductivity, K / m d⁻¹					
PT1	3.5	3.3	2.6	3.7	—	—
PT2	4.1	3.2	3.3	4.0	—	—
PT3*	6.0	6.3	2.9	10.4	—	—
PT4	6.2	3.6	4.5	5.6	—	—
	Estimated storativity, S_{est}					
PT1	4.65×10^{-2}	—	6.03×10^{-2}	4.81×10^{-2}	5.13×10^{-2}	1.06
PT2	1.03×10^{-2}	—	1.18×10^{-2}	1.22×10^{-2}	1.14×10^{-2}	1.06
PT3*	3.08×10^{-3}	—	3.68×10^{-3}	8.42×10^{-3}	4.57×10^{-3}	1.27
PT4	3.51×10^{-3}	—	3.72×10^{-3}	3.94×10^{-3}	3.72×10^{-3}	1.03

* Low confidence. § Geometric standard deviation factor.

Table 8. Hydraulic parameters determined for piezometre DCP1.

Pumping test	Theis draw-down	Theis re-covery	Agarwal recovery	Modified Agarwal recovery	Geometric average	GSDF§
	Effective transmissivity, T_{eff} / m² d⁻¹					
PT1	8.1	6.8	7.1	7.9	7.4	1.07
PT2	6.9	5.5	5.8	6.6	6.1	1.10
PT3*	11.0	5.8	3.1	18.7	7.8	1.96
PT4	14.1	7.5	7.4	9.7	9.3	1.30
	Hydraulic conductivity, K / m d⁻¹					
PT1	6.6	5.5	5.8	6.4	—	—
PT2	5.6	4.4	4.7	5.4	—	—
PT3*	9.0	4.8	2.5	15.2	—	—
PT4	11.5	6.1	6.0	7.9	—	—
	Estimated storativity, S_{est}					
PT1	2.53×10^{-3}	—	3.81×10^{-3}	3.32×10^{-3}	3.17×10^{-3}	1.14
PT2	3.71×10^{-3}	—	3.21×10^{-3}	3.72×10^{-3}	3.54×10^{-3}	1.03
PT3*	1.49×10^{-3}	—	1.51×10^{-3}	1.03×10^{-2}	2.85×10^{-3}	1.83
PT4	3.42×10^{-3}	—	1.09×10^{-2}	7.19×10^{-3}	6.45×10^{-3}	1.44

* Low confidence. § Geometric standard deviation factor.

Table 9. Hydraulic parameters determined for piezometre DCP2.

Pumping test	Theis drawdown	Theis re-covery	Agarwal recovery	Modified Agarwal re-covery	Geometric average	GSDF§
	Effective transmissivity, T_{eff} / m² d⁻¹					
PT1	6.7	3.9	4.8	6.6	5.3	1.26
PT2	8.5	6.3	6.3	7.2	7.0	1.14
PT3*	11.2	4.9	2.7	17.0	7.1	2.04
PT4	12.5	7.0	7.1	9.9	8.8	1.28
	Hydraulic conductivity, K / m d⁻¹					
PT1	5.5	3.1	3.9	5.4	—	—
PT2	7.0	5.1	5.1	5.9	—	—
PT3*	9.1	4.0	2.2	13.9	—	—
PT4	10.1	5.7	5.8	8.1	—	—
	Estimated storativity, S_{est}					
PT1	3.33×10^{-3}	—	4.23×10^{-3}	3.43×10^{-3}	3.64×10^{-3}	1.05
PT2	2.65×10^{-3}	—	4.92×10^{-3}	4.47×10^{-3}	3.87×10^{-3}	1.25
PT3*	2.08×10^{-3}	—	1.30×10^{-3}	1.27×10^{-2}	3.25×10^{-3}	2.15
PT4	—	—	—	—	—	—

* Low confidence. § Geometric standard deviation factor.

Table 10. Hydraulic parameters determined for piezometre C1.*

Pumping test	Theis drawdown	Theis re-covery	Agarwal recovery	Modified Agarwal re-covery	Geometric average	GSDF§
	Effective transmissivity, T_{eff} / m² d⁻¹					
PT1	19.8	6.9	9.4	16.6	12.1	1.53
PT2	37.0	15.9	25.3	17.1	22.5	1.40
PT3	25.1	6.7	4.9	58.2	14.8	2.72
PT4	39.5	9.2	13.1	29.4	19.3	1.80
	Hydraulic conductivity, K / m d⁻¹					
PT1	16.2	5.6	7.7	13.5	—	—
PT2	30.2	13.0	20.6	14.0	—	—
PT3	20.5	5.5	4.0	47.5	—	—
PT4	32.2	7.5	10.7	23.9	—	—
	Estimated storativity, S_{est}					
PT1	1.57×10^{-3}	—	4.59×10^{-3}	4.41×10^{-3}	3.16×10^{-3}	1.51
PT2	9.03×10^{-3}	—	6.29×10^{-3}	3.80×10^{-3}	6.00×10^{-3}	1.27
PT3	3.71×10^{-3}	—	1.50×10^{-3}	2.23×10^{-2}	4.99×10^{-3}	2.87
PT4	2.19×10^{-2}	—	1.90×10^{-2}	1.05×10^{-2}	1.63×10^{-2}	1.19

* Low confidence. § Geometric standard deviation factor.

Reassuringly, for a given piezometre and pumping test, the four methods tend to produce results that are in very good agreement with each other, with both transmissivity and storativity values almost always in the same orders of magnitude; the geometric standard deviation factors never exceed 1.30 and 1.44, respectively. However, unsurprising exceptions to this are the results for pumping test 3, and the results at C1 for all pumping tests. The trivial level of drawdown produced in both cases, on top of considerably greater variance in the hydraulic head signal detected at C1 which produced linear regressions of considerably worse quality (see R^2 values in Appendix, figures A.6, A.13, A.21, and A.29) imply there is much less confidence in the validity of these results and will mostly be disregarded in the subsequent comparisons.

According to work by Trabucchi *et al.* (2018), the Agarwal recovery method works best when the duration of pumping is at least 10 times greater than the characteristic time, t_c, for the piezometre being studied.

$$t_c = \frac{r^2 S}{T} \tag{30}$$

This condition is met in all piezometres except A3. As listed in Table 11, for the three pumping tests in which it was possible to estimate, t_c at A3 is always at least 9 min too long. Moreover, none of the piezometres meet this condition for pumping test 3, but once again is simply attributed to the anomalous pumping duration.

However, in the present study, the hydraulic parameter estimates produced at point A3 using the Agarwal method are not so different from those calculated using the other methods. In fact, the results are particularly close to those generated using the Theis recovery method, indicating that the Agarwal method is valid for this study.

Table 11. Characteristic time, t_c, calculated for each piezometre and pumping test, all values expressed in unit of minutes.

Piezometre	PT1	PT2	PT3*	PT4
A3	26.7	28.9	—	32.0
B1	4.5	4.8	14.4	4.1
BCP1	9.7	0.9	14.3	4.5
BCP2	7.4	5.6	15.3	7.3
DCP1	4.3	8.5	12.5	0.7
DCP2	6.8	4.0	17.3	0.0
C1	4.1	12.8	25.7	7.6

* Low confidence.

Upon inspection of the reliable effective transmissivities, it stands out that they all lie within a small range (1.9-14.1 $m^2 d^{-1}$), even when comparing across all piezometres, all pumping tests, and all methods. This range of orders of magnitude (10^0-10^1) places the aquifer right on the threshold between somewhat permeable and permeable (Custodio and Llamas, 1983), and is completely in line with what is predicted by the empirical relationship between granulometry (in this case 0.1-0.2 mm) and permeability. Moreover, as explained in Section 2.4, the inherent imprecision of the method means that within this type of range, the transmissivities estimated can be considered to be practically identical, which is also in line with what is expected given the nature of effective transmissivity as an integrated value of all local transmissivities, and the homogeneous design of the aquifer.

Comparing the estimated coefficients of storativity across piezometres, these are slightly more variable than the effective transmissivities, as is expected given what it physically represents (see Section 2.4). However, this variability is not large, with a total range of 0.129-6.03 x 10^{-2}, or 10^{-3}-10^{-2} in terms of order of magnitude, which again reflects the high homogeneity of the aquifer being studied.

In comparing the storativities obtained, it is more pertinent to discuss them in qualitative terms, rather than quantitative, since what matters is the degrees of hydraulic connectivity of

the different points of the aquifer relative to each other. The results of this analysis are illustrated in figures 15 to 17, which show lines emanating from the pumping piezometre and toward the observation piezometres. The thickness of each line is directly proportional to the degree of connectivity between the two points, determined by the coefficient of storativity obtained for that connection using the Agarwal method. This method was chosen given its proven reliability and robustness, both in this work and in previous ones (Trabucchi *et al.*, 2018; Martinez-Landa *et al.*, 2021). Additionally, a diagram integrating all the information from the previous ones is shown in Figure 18.

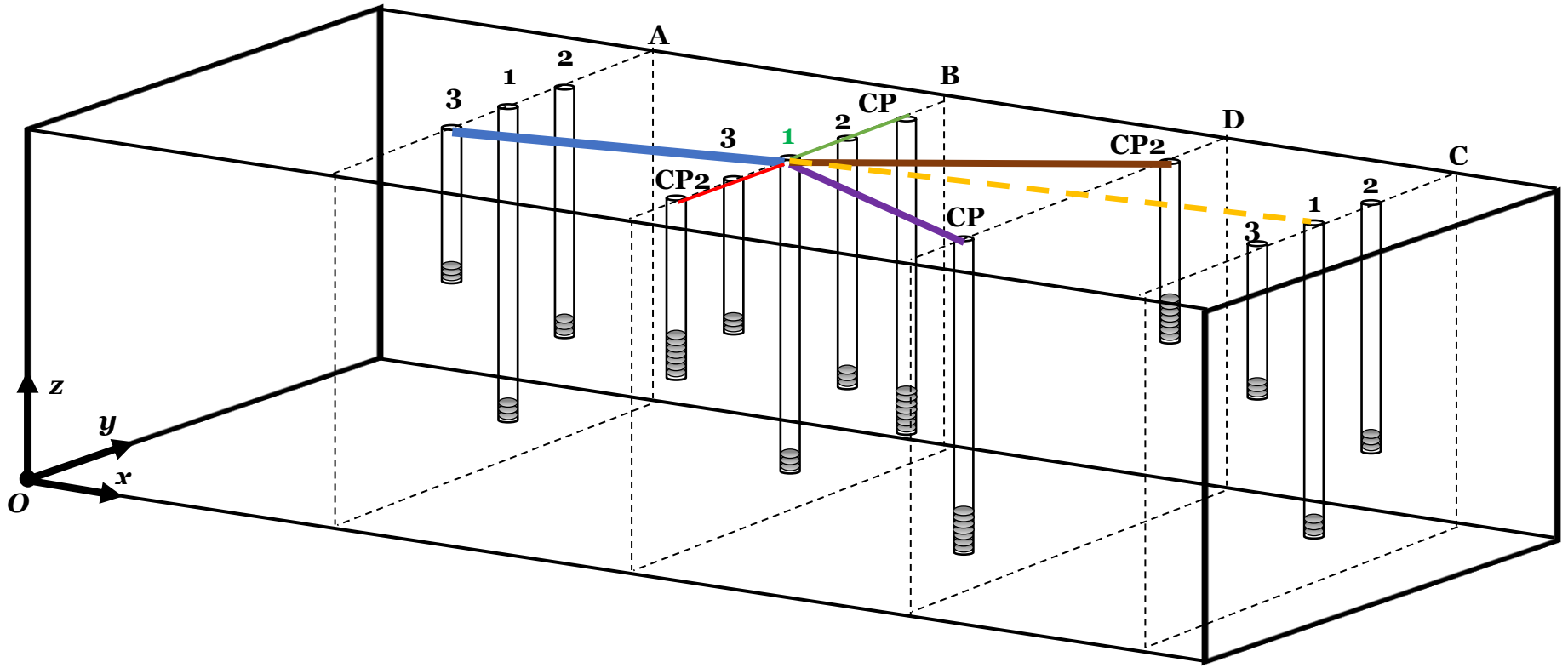

Figure 15. Oblique projection of the artificial aquifer system with lines illustrating the degree of hydraulic connectivity generated from PT1. Line thickness is directly correlated to the magnitude of the estimated storativity coefficient, S_{est}, calculated by the Agarwal recovery method. The dashed line employed for C1 is used to signal lower confidence in this estimate.

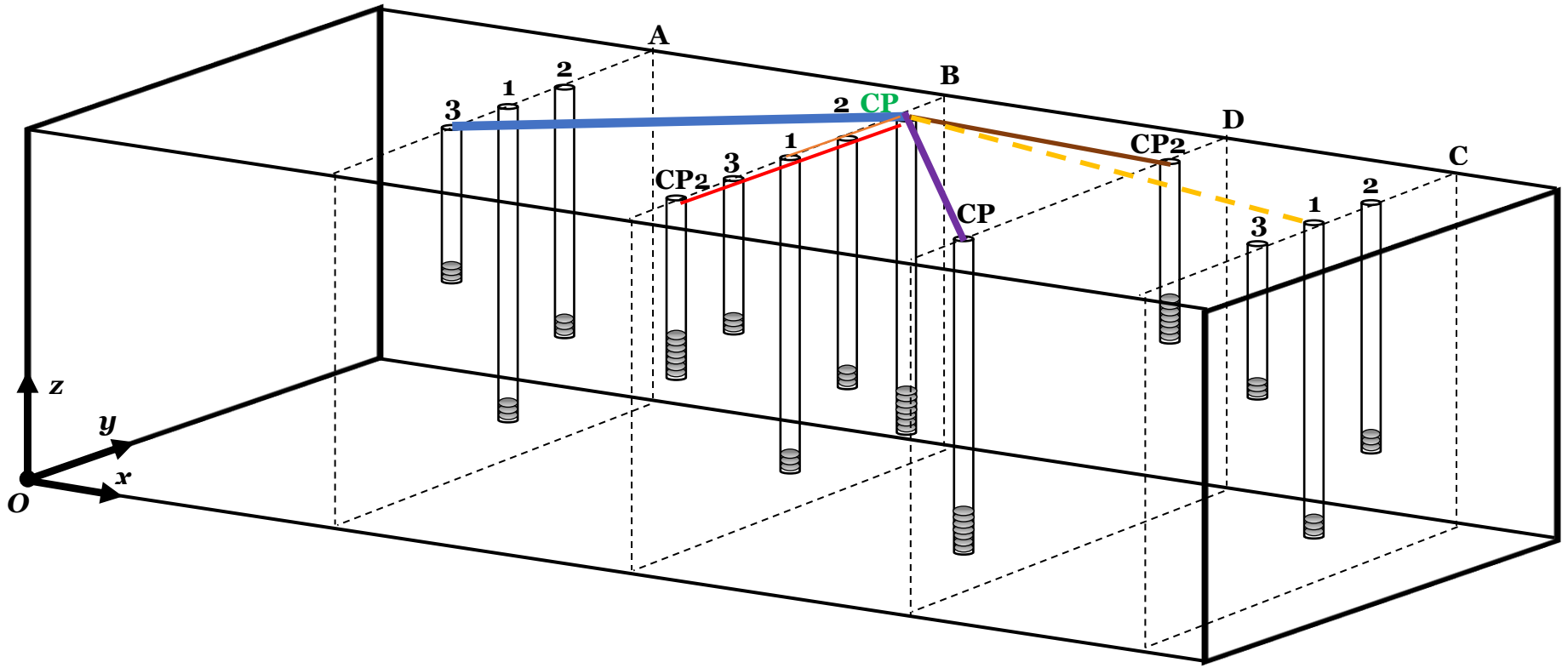

Figure 16. Oblique projection of the artificial aquifer system with lines illustrating the degree of hydraulic connectivity generated from PT2. Line thickness is directly correlated to the magnitude of the estimated storativity coefficient, S_{est}, calculated by the Agarwal recovery method. The dashed line employed for C1 is used to signal lower confidence in this estimate.

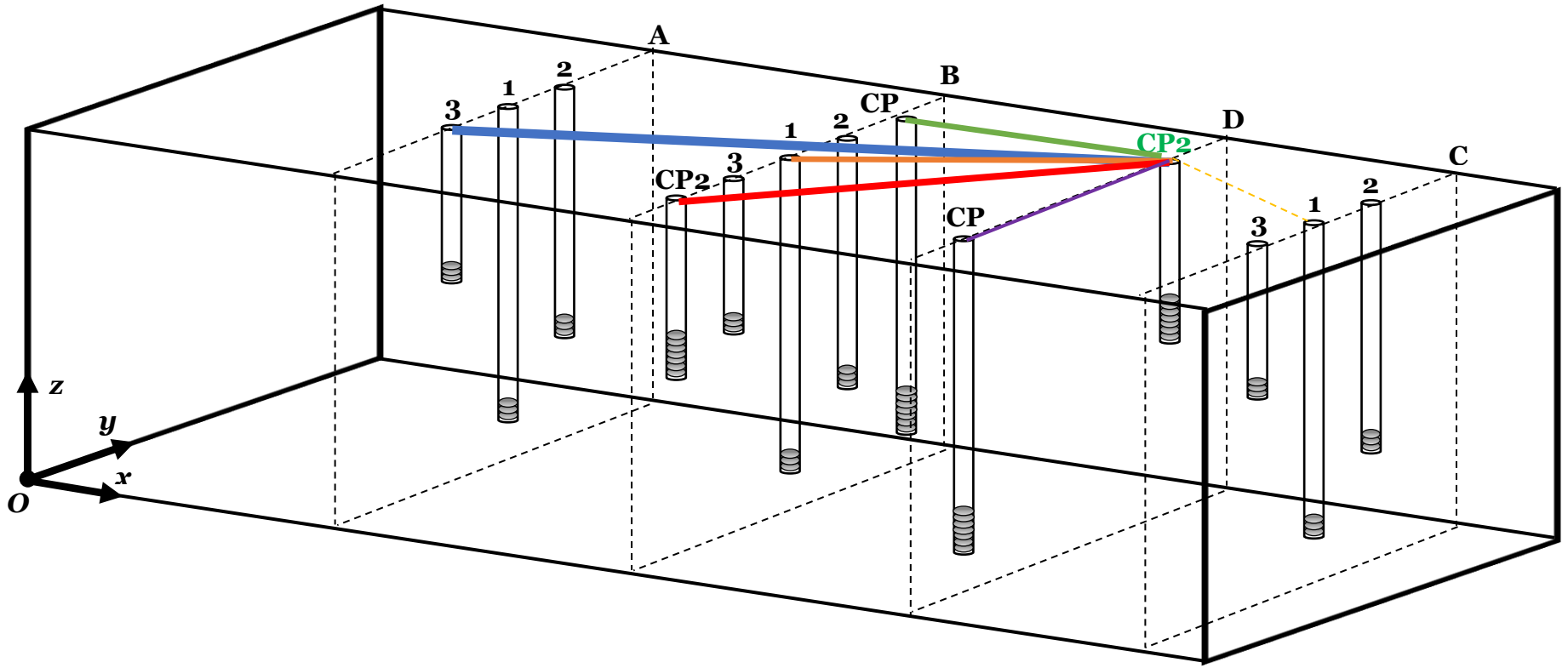

Figure 17. Oblique projection of the artificial aquifer system with lines illustrating the degree of hydraulic connectivity generated from PT4. Line thickness is directly correlated to the magnitude of the estimated storativity coefficient, S_{est}, calculated by the Agarwal recovery method. The dashed line employed for C1 is used to signal lower confidence in this estimate.

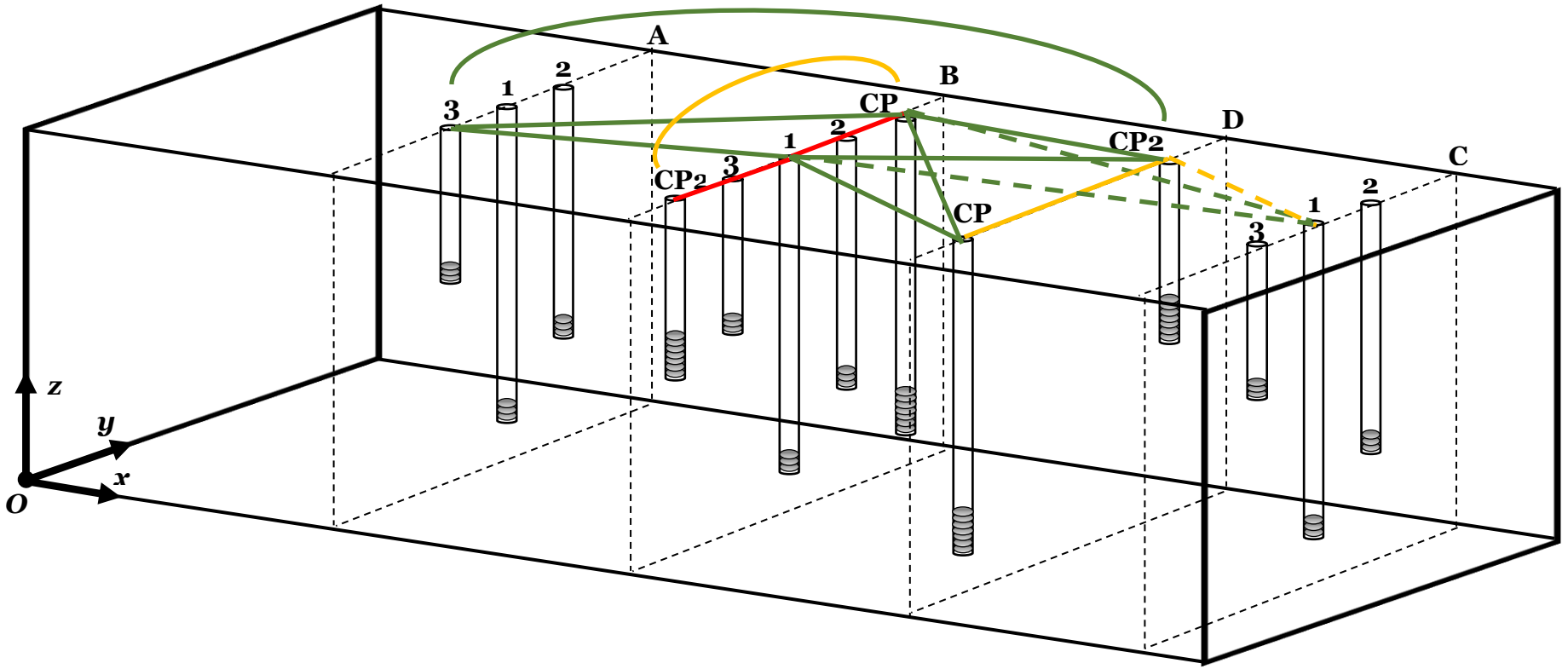

Figure 18. Oblique projection of the artificial aquifer system with lines illustrating the degree of hydraulic connectivity between all the piezometres probed. The dashed lines employed for C1 are used to signal lower confidence in these estimates.

The first impression the diagram in Figure 18 gives is that the hydraulic connectivity in the pilot aquifer is largely good: the green lines dominate over the yellow and red lines. In addition, the good connectivity is mostly longitudinal, the instances of poor connectivity are almost all within the same cross-section: B1-BCP1, B1-BCP2, BCP1-BCP2, DCP1-DCP2. The only other case of poor connectivity is DCP2-C1, which corroborates the conjecture made in Section 3.1.1 based on the lower drawdown response in C1 from extraction in DCP2 with respect to B1. Interestingly, the rest of the diagonal connections (*e.g.*, A3-B1, B1-DCP1, B1-DCP2) show relatively excellent hydraulic connectivity. The case of A3 is especially noteworthy, which displays high connectivity with all the points probed, including DCP2, which is a considerable distance away (in the context of this artificial aquifer). Another feature which comes to attention is the greater connectivity in BCP1-BCP2 than B1 with either of the two, despite lying between them. This suggests there is a preferential pathway that circumvents the point where B1 is placed.

Table 12 presents the storativity information used to create the diagrams for each pumping test, with the piezometres listed in ascending order of S_{est}, and therefore descending degree of connectivity.

Table 12. Summary of the estimated and normalised coefficients of storativity estimated via the Agarwal recovery method.

PT1 (B1)			**PT2 (BCP1)**			**PT4 (DCP2)**		
Pz	S_{est}	$S_{est\text{-}norm}$	Pz	S_{est}	$S_{est\text{-}norm}$	Pz	S_{est}	$S_{est\text{-}norm}$
A3	2.46×10^{-3}	0.04	A3	2.07×10^{-3}	0.03	A3	1.29×10^{-3}	0.02
DCP1	3.81×10^{-3}	0.06	DCP1	3.21×10^{-3}	0.05	BCP2	3.72×10^{-3}	0.06
DCP2	4.23×10^{-3}	0.07	DCP2	4.92×10^{-3}	0.08	B1	5.14×10^{-3}	0.09
C1	4.59×10^{-3}	0.08	C1	6.29×10^{-3}	0.10	BCP1	5.19×10^{-3}	0.09
BCP1	6.02×10^{-2}	0.99	BCP2	1.17×10^{-2}	0.19	DCP1	1.09×10^{-2}	0.18
BCP2	6.03×10^{-2}	1.00	B1	4.33×10^{-2}	0.72	C1	1.90×10^{-2}	0.31

3.2 Dissolved oxygen

The concentrations of dissolved oxygen at piezometres A3, B1, BCP1, and DCP2 and at various depths are plotted against time in figures 19 to 22. The time series is approximately 12 days long, beginning 6 days prior to the first pumping test and ending almost 6 days later, with t = 0 defined as the start of PT1. The basis for including this pre-pumping period is to observe the natural trends that the dissolved oxygen follows, and therefore be more confident in attributing any changes as a response to pumping. The data that were smoothed using the Savitzky-Golay filter are plotted as opaque lines, and the original datasets are plotted alongside them but with a degree of transparency.

It bears mentioning that the data collected for $t < 0$ was done so with a measurement frequency of 30 min, rather than the 5 s which was used for $t \geq 0$. This was done to keep the quantity of data more manageable, but also implies that those natural trends will be more washed out as compared to the data with greater measurement frequency.

Each line of the oxygen plots corresponds to a different sensor, each of which is placed at a different depth. They are identified, however, by their height with respect to the base of the tank in order to set them in the same reference system as the hydraulic head. Therefore, sensors labelled '0.05 m' are those closest to the base (1.35 m below ground surface), and those labelled '1.15 m' are furthest from the base (0.25 m below ground surface).

In those cases where the oxygen signal became erratic and was no longer conveying credible information, the lines have been truncated. In other cases, the sensor did not function adequately at any point, and the entire dataset has been omitted.

Each figure includes a plot of the hydraulic head for the piezometre adjacent to the given set of oxygen sensors, as well as a plot of precipitation as registered by the weather station installed at the pilot plant. The time series are fully aligned to allow comparing events with time resolution.

It is also important to remember that each sensor is a small polymer-coated metal tip, thus the data it generates is best understood as a point reading, and not necessarily representative of a large aquifer volume.

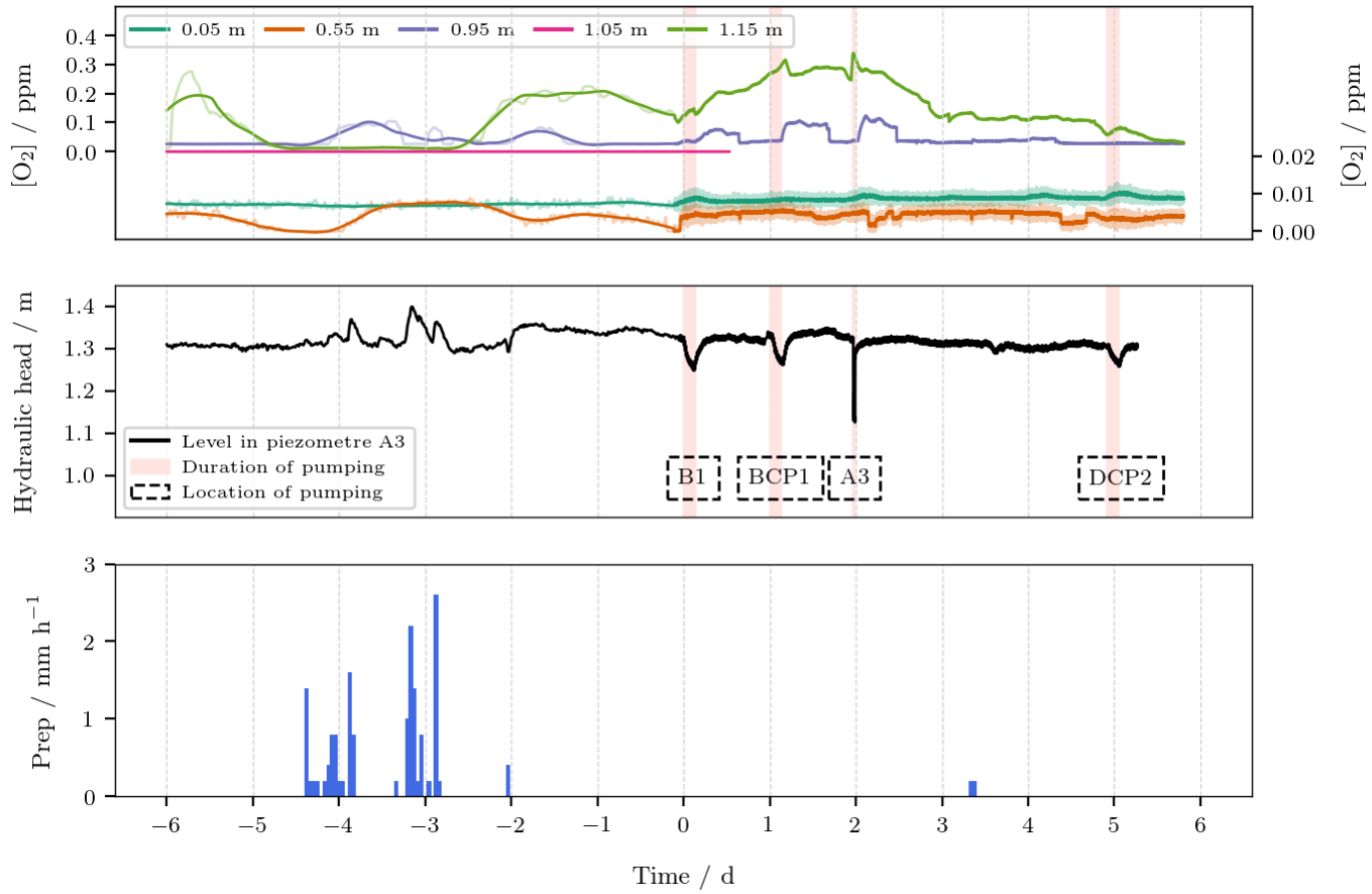

Figure 19. (Top) Temporal evolution of the dissolved oxygen concentration at five heights, *z*, above the base of the tank in an area immediately adjacent to piezometre A3. The sections highlighted in soft red represent the time in which pumping of groundwater occurred. (Middle) Temporal evolution of the hydraulic head in piezometre A3. (Bottom) The precipitation that occurred during the time in which the study was carried out. The negative times represent the time prior to the first pumping test, $t = 0$ is defined as the moment the first pumping test began.

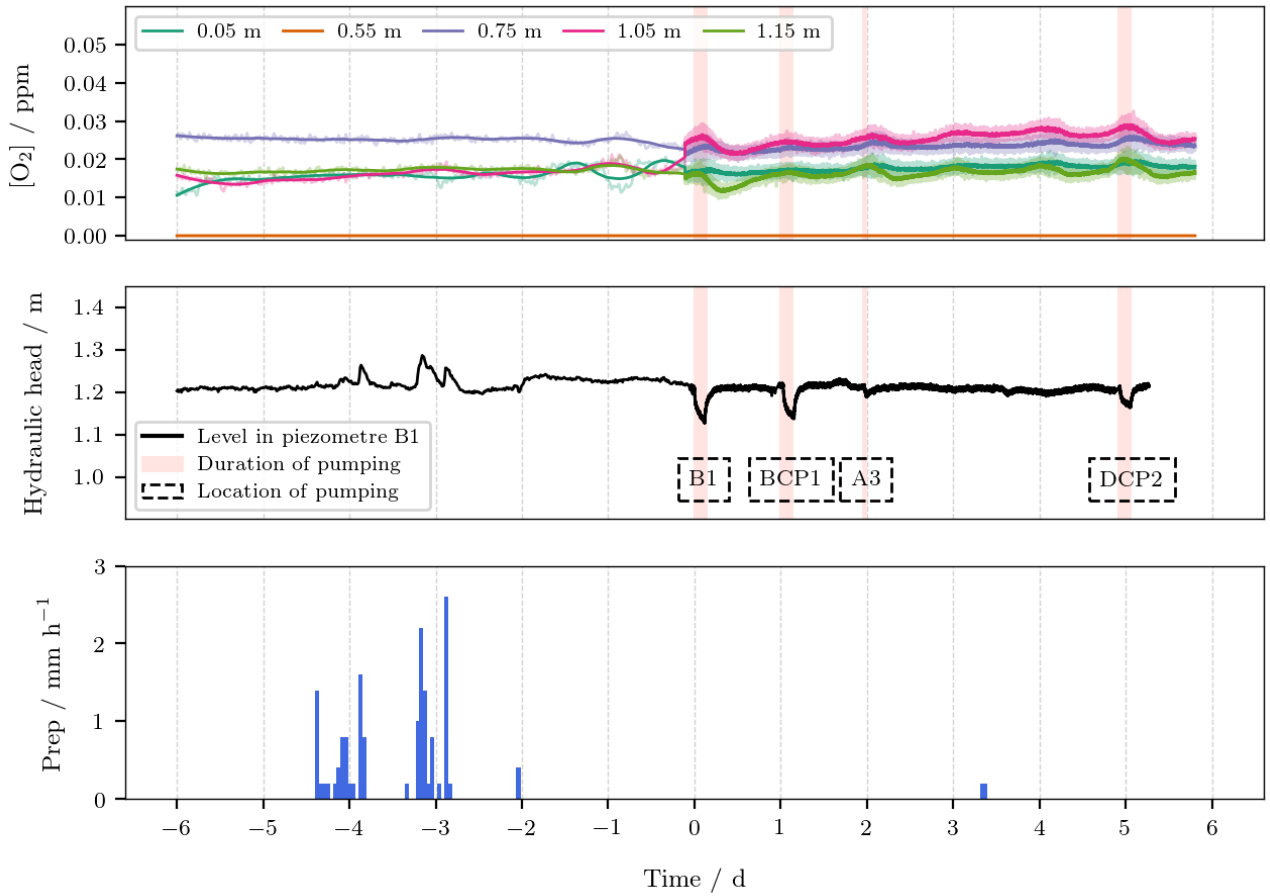

Figure 20. (Top) Temporal evolution of the dissolved oxygen concentration at five heights, *z*, above the base of the tank in an area immediately adjacent to piezometre B1. The sections highlighted in soft red represent the time in which pumping of groundwater occurred. (Middle) Temporal evolution of the hydraulic head in piezometre B1. (Bottom) The precipitation that occurred during the time in which the study was carried out. The negative times represent the time prior to the first pumping test, $t = 0$ is defined as the moment the first pumping test began.

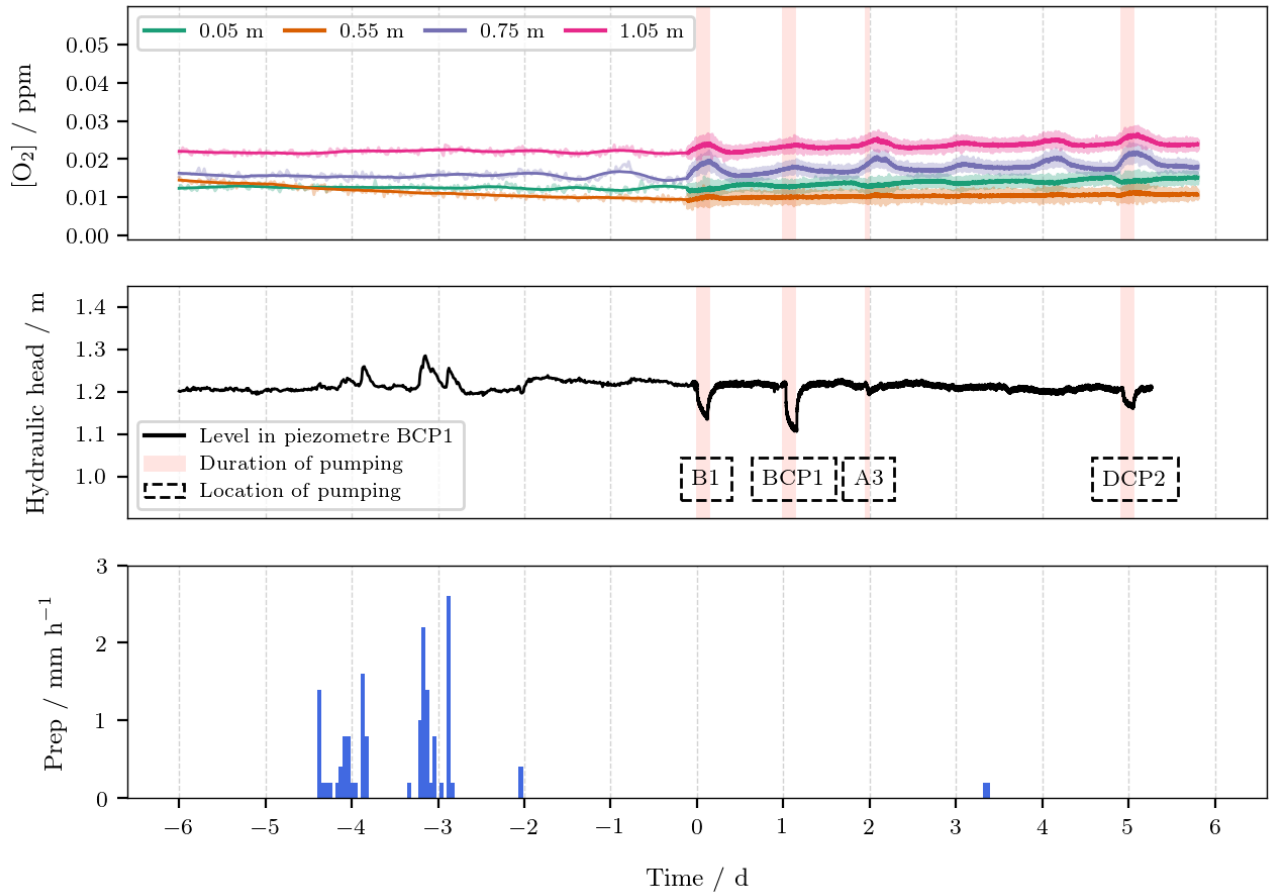

Figure 21. (Top) Temporal evolution of the dissolved oxygen concentration at five heights, *z*, above the base of the tank in an area immediately adjacent to piezometre BCP1. The sections highlighted in soft red represent the time in which pumping of groundwater occurred. (Middle) Temporal evolution of the hydraulic head in piezometre BCP1. (Bottom) The precipitation that occurred during the time in which the study was carried out. The negative times represent the time prior to the first pumping test, $t = 0$ is defined as the moment the first pumping test began.

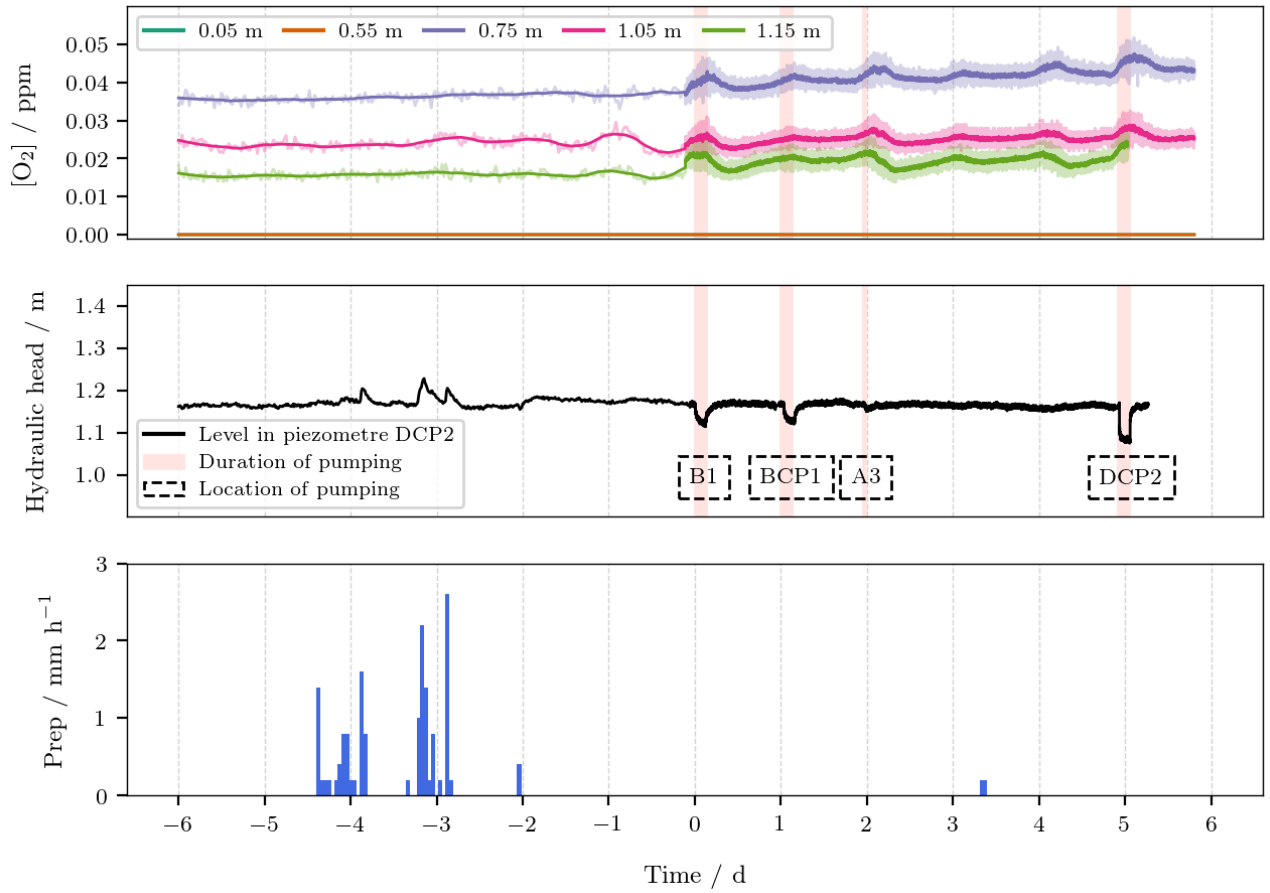

Figure 22. (Top) Temporal evolution of the dissolved oxygen concentration at five heights, *z*, above the base of the tank in an area immediately adjacent to piezometre DCP2. The sections highlighted in soft red represent the time in which pumping of groundwater occurred. (Middle) Temporal evolution of the hydraulic head in piezometre DCP2. (Bottom) The precipitation that occurred during the time in which the study was carried out. The negative times represent the time prior to the first pumping test, t = 0 is defined as the moment the first pumping test began.

3.2.1 Oxygen at A3

Of all the twenty sensors, the one at z = 0.95 m of piezometre A3 (Figure 19) produced the most straightforward results to interpret. The peaks at t = −4 and −3 d follow periods of oxygen-rich precipitation, although there is a slight delay between the rain falling and the rise in dissolved oxygen concentration. This lag is likely due to the travel time of the water through the somewhat permeable porous medium to a depth of 0.45 m, where the sensor was placed. The peaks following pumping for PT1, PT2, and PT3 are also slightly delayed with respect to the start of the perturbation. The increase in oxygen concentration could be attributed to the negative pressure exerted by the extraction of groundwater, which would pull gaseous-phase particles, including oxygen, into the groundwater. These rises are rapid and reach a fairly steady state for several hours, then the level falls back to the initial value in a similarly quick fashion. In absolute terms, the rises are insignificant, going from close to 0 to 0.1 ppm.

On the other hand, the behaviour of the signal at z = 1.15 m is complicated to decipher. The irregularity of the oscillation in the pre-pumping period does not lend itself to any evident explanation, the sustained rise starting at $t \approx -2.5$ d could be due to the precipitation, but it is curious that it would respond later to this perturbation than the sensor at z = 0.95 m (which first responded around t = −4 d), despite being closer to the ground surface. Then, the signal appears to rise concomitantly with the first pumping test, although this rise in oxygen concentration actually begins before pumping, so it does not appear that the pumping is the reason behind the rise initiating. Pumping during PT3 and PT4 does appear to shortly precede small rises in concentration. Overall, it is difficult to assign a simple relationship between pumping and oxygen concentration at z = 1.15 m.

Of the sensors at A3 that show non-zero readings, the two deepest (z = 0.05, 0.55 m) consistently read the lowest concentrations, which is not an unexpected result given that oxygen concentration tends to decrease with depth below surface. At z = 0.55 m, there is a small amplitude (< 0.0075 ppm) oscillation with a period of approximately 4 days seen during pre-pumping ($-6 < t < -2$), indicating some natural fluctuation, although clearly minuscule, but there is little to no clear response from pumping. At z = 0.05 m, no natural trends prior to pumping are observed, and some small peaks are produced that coincide in time with the pumping tests, especially PT1, PT3 and PT4. Once again, however, these rises (< 0.001 ppm) are practically negligible in absolute terms.

At z = 1.05 m, the sensor produced negative readings, which is interpreted as anoxicity (0 ppm).

3.2.2 Oxygen at B1

In this instance, there is another case of a sensor reporting anoxicity, but this time at a greater depth (z = 0.55 m). Somewhat oddly, the oxygen concentrations reported at the deepest point (z = 0.05 m) and the shallowest point (z = 1.15 m) are practically identical, approximately 0.017 ppm. The full range of oxygen concentrations between the four sensors not reading 0 is approximately 0.010-0.025 ppm.

Mild fluctuations in oxygen concentrations are visible in these same four sensors in the time prior to pumping, becoming especially noticeable from t = −2 d and at z = 0.05 and 1.05 m. From the start of pumping at t = 0, the concentrations present transverse wave-like patterns. The sensors can be categorised into two groups based on the similarity in amplitudes: 1) z = 1.15 and 1.05 m; and 2) z = 0.05 and 0.75 m. The first group presents generally higher amplitude, especially following PT1 and PT4, but peaks can be identified on each day. This includes the two days without pumping (t = 3, 4 d), which could suggest that the oscillations in oxygen concentrations are independent of pumping. However, across all four sensor readings, the amplitudes are clearly greater on the days with pumping than those without, thus it is more likely that the pumping does create a response in the concentration and is at least partly responsible for the change in signal on those days.

The periodicity and phase of the four lines are constant and quite similar, with peaks and troughs centred at $t \approx$ 0.1, 1.1, *etc.* and $t \approx$ 0.6, 1.6, *etc*, respectively. In terms of time of day, these correspond to approximately 13:00 and 01:00. It could be enlightening to investigate, in further work, what these times coincide with which could help explain this behaviour in dissolved oxygen concentration.

3.2.3 Oxygen in BCP1

The oxygen concentrations in this location behave quite similarly to those discussed in B1, and they can also be described as transverse wave-like. Also, the sensors can again be categorised into two groups based on their amplitudes: 1) z = 0.75 and 1.05 m; and z = 0.05 and 0.55 m. The first group has larger rises of approximately 0.002 ppm, *c*ompared with around 0.0001 ppm for the second. The concentrations range from 0.010 to 0.025 ppm, matching B1. Oddly, the signal at z = 0.05 m appears to be almost fully out of phase with the other three. Where the majority show peaks and troughs at about the same time

as those seen in B1 ($t \approx 0.1, 1.1, \ldots$, and $t \approx 0.6, 1.6, \ldots$, respectively), the oxygen concentration displays troughs and peaks.

The relationship between pumping and dissolved oxygen which is hinted by this plot is the same as that identified in B1, namely that pumping causes a slightly greater increase in oxygen concentration compared to no pumping, but small rises certainly occur even in its absence.

3.2.4 Oxygen in DCP2

In this location, the two deepest sensors ($z = 0.05, 0.55$ m) recorded anoxicity throughout the period studied, while the next deepest ($z = 0.75$ m) recorded the highest levels ($\approx$ 0.038 ppm). The non-anoxic points display acutely similar patterns, both in terms of amplitude and periodicity, are fully in phase, and range in values from 0.018 to 0.038 ppm. Just like in the other piezometre locations, the tallest peaks coincide with PT1, PT3, and PT4.

Consistent with the rest, the pumping-dissolved oxygen relationship suggested by this data is one of slight positive correlation, while acknowledging that small peaks also occur on the days where pumping was not carried out.

It is noteworthy that not a single DO sensor in B1, BCP1, or DCP2 produced a response to the precipitation that occurred on $t = -4$ and -3, and in A3 only the sensor at $z = 0.95$ m gave a DO response that can be ascribed with some confidence to the precipitation.

3.2.5 DO behaviour across the aquifer system

The behaviour which would be expected of this system would be for the DO levels to be higher in the water closest to the recharge point (section A) and steadily decrease since oxygen is preferentially consumed in the oxidation of organic matter as it travels across the porous medium, reaching a minimum at the point closest to discharge (section D). Nevertheless, this is not observed, instead, the sensors at point DCP2 registered the highest average DO levels, discounting the values at A3/$z = 1.15$ which were higher than at DCP2 but also relatively unstable.

As described in Section 1.5, the processes involved in DO concentration in soil and groundwater are diverse and interact in complicated ways. However, it is not far-fetched to assume that the majority of the DO registered at point A3 originates from aeration of

the water as it is recharged into the aquifer system. This would explain why the concentration gradient is not simply negative with respect to depth, as is typically expected given the role of the atmosphere as a source of oxygen. Instead, there is an uneven distribution, with apparently high and volatile levels at the superficial point (A3/z = 1.15), anoxicity in the next point (A3/z = 1.05), and a non-zero value at the deepest point (A3/z = 0.05). As the water travels through the aquifer system and the oxygen is consumed in biodegradation reactions, the DO concentration is predicted to decrease. This is not witnessed between sections A and B, and indeed, as stated, the highest levels of DO are actually encountered in section D, strongly suggesting that other processes are taking place that are replenishing the levels of DO. However, the two deepest points probed in DCP2 show anoxicity, the only location where this is found. This could be an indication that DO is indeed being consumed by organic matter reduction; however, the upper layers are having that oxygen replenished by processes such as diffusion from the atmosphere and photosynthesis from plants, processes which do not affect the lower layers.

The points of the artificial aquifer system that were probed can be classified as being under anaerobic conditions, since they all showed DO concentrations below 1 ppm (USGS, 2006), and four separate points were even fully anoxic (0 ppm). Therefore, it is likely that other terminal electron acceptors, , such as sulfate, nitrate, or manganese, are more significant in the reduction of the organic contaminants being carried in the partially-treated wastewater. Ascertaining which of these alternative electron acceptors are present and playing a more significant role in biodegradation could be done by measuring the redox potential, because each species is associated with a unique range of redox potential, as explained in Section 1.5.

4. Conclusions & further work

In this work, the hydraulic characteristics of a pilot MAR-SAT system located in Palamós have been determined. This has been done as a prior medium characterisation for chaotic flow experiments to be performed by the Hydrogeology Research Group (UPC-CSIC). Through the implementation of a hydraulic tomography involving four separate pumping tests, it has been established that the homogeneous artificial aquifer installed in tank 1 has a hydraulic conductivity, K, in the range of 10^{0}-10^{1} m d^{-1}, which classifies it as a "somewhat permeable" to "permeable" porous medium, as defined by consensus of the hydrogeological community. This range of hydraulic conductivity is coherent with the grain-size of the particles that compose the aquifer (0.1-0.2 mm) according to the empirical relationship established between the two. Furthermore, the relative hydraulic connectivity between various points were ascertained via the coefficients of storativity, which reveal that there is good connectivity longitudinally, *i.e.*, from cross-section A to B, B to D, *etc.*, but not so in the transverse direction, *i.e.*, within a given cross-section.

The importance of dissolved oxygen in the biodegradation of organic contaminants motivated a simultaneous study of its levels across the tank. Time-resolved DO concentrations for four sites in the artificial aquifer have been obtained, with five depths probed at each site. The values registered during the period of observation never surpassed 0.4 ppm, and in the majority of cases did not even reach 0.03 ppm, which firmly places these sites as anaerobic.

Fluctuations in DO concentrations are perceptible, but generally very small. A regular pattern of a peak around 13:00 and a trough at 01:00 is observed in most of the sites, features which are slightly intensified on the days on which pumping took place. Nevertheless, this is the only effect that can be ascribed with some confidence to the pumping, there is no other obvious impact that can be reported. Similarly, it has not been possible to identify a relationship between the relative hydraulic connectivities and DO levels.

To further develop our understanding of the biodegradation processes occurring in this artificial aquifer, an examination of the redox potential across the system would be helpful in identifying the terminal electron acceptors present and therefore which dominate the degradation process. Moreover, in terms of the hydraulics of the system, diagnostic plots could be elaborated to improve the conceptual understanding of the aquifer characteristics, which would aid in determining if the model chosen to describe it is valid, or if another model is more appropriate.

Finally, the broad objective of this thesis was to contribute to the task of addressing water scarcity by engaging with two of the targets listed in the Sustainable Development Goals, specifically those regarding the guarantee of wastewater treatment, safe reuse, and ensuring the supply of freshwater. The solution chosen for study, managed aquifer recharge coupled to soil-aquifer treatment (MAR-SAT), and water reclamation more broadly, have an enormous potential to aid in achieving these targets. If properly implemented, they can contribute to wastewater treatment in a relatively cost-effective manner, improve water quality, store water for later recovery, *etc.*

Despite this host of benefits, uptake of water reclamation is low; one estimate places the proportion of wastewater reclaimed in the EU at 2% (Water Reuse Europe, 2018). This is attributed to factors like lack of harmonised regulations on quality standards, and social rejection. The former is starting to be addressed, with the EU publishing its first regulation regarding the issue (Regulation (EU) 2020/741), although it only envisages its use for agriculture, overlooking all the other potential uses. The latter, on the other hand, does not have straightforward solutions. It has been repeatedly demonstrated that consumers overwhelmingly reject reclaimed water on the basis of uncleanliness (Menegaki *et al.*, 2007; Bakopoulou *et al.*, 2008; Hui & Cain, 2017). This is yet another demonstration that for engineering solutions to be successful, it is crucial for social aspects to be included in the scope of the project, such as building trust in the public.

References

A/RES/70/1 (2015) *Transforming our world: The 2030 agenda for sustainable development*. Available at: https://sustainabledevelopment.un.org/content/documents/21252030 Agenda for Sustainable Development web.pdf.

ACA (2022) 'Palamós (DPAM)'. Available at: https://aca.gencat.cat/web/.content/20_Aigua/02_infraestructures/05_estacions_depuradores_daigues_residuals/Fitxes_EDAR/DPAM_Fitxa_web_EDAR.pdf.

ACA (no date) *Regeneració*. Available at: https://aca.gencat.cat/ca/laigua/gestio-del-cicle-de-laigua/regeneracio/ (Accessed: 2 September 2022).

Agarwal, R. G. (1980) 'A new method to account for producing time effects when drawdown type curves are used to analyze pressure buildup and other test data', in *SPE Annual Technical Conference and Exhibition*. doi: 10.2118/9289-ms.

Ahmadi, N. *et al.* (2022) 'Oxygen Propagation Fronts in Porous Media Under Evaporative Conditions at the Soil/Atmosphere Interface: Lab-Scale Experiments and Model-Based Interpretation', *Water Resources Research*, 58(6), p. e2021WR031668. doi: 10.1029/2021wr031668.

AMB (no date) *ERA del Prat de Llobregat*. Available at: https://www.amb.cat/web/ecologia/aigua/instalacions-i-equipaments/detall/-/equipament/era-del-prat-de-llobregat/360457/11818 (Accessed: 16 September 2022).

Asano, T. and Cotruvo, J. A. (2004) 'Groundwater recharge with reclaimed municipal wastewater: Health and regulatory considerations', *Water Research*, 38(8), pp. 1941–1951. doi: 10.1016/j.watres.2004.01.023.

Bagtzoglou, A. C. and Oates, P. M. (2007) 'Chaotic Advection and Enhanced Groundwater Remediation', *Journal of Materials in Civil Engineering*, 19(1), pp. 75–83. doi: 10.1061/(asce)0899-1561(2007)19:1(75).

Bakopoulou, S. *et al.* (2008) 'Using recycled water for agricultural purposes in the Thessaly region, Greece: A primary investigation of citizens' opinions', *WIT Transactions on Ecology and the Environment*, 109, pp. 869–878. doi: 10.2495/WM080881.

Bauer, R. D. *et al.* (2009) 'Enhanced biodegradation by hydraulic heterogeneities in petroleum hydrocarbon plumes', *Journal of Contaminant Hydrology*. Elsevier B.V., 105(1–2), pp. 56–68. doi: 10.1016/j.jconhyd.2008.11.004.

Bernis, M. (2022) 'Canvi climàtic: cal preparar-se per viure amb menys aigua', *Diari ARA*, 30 July. Available at: https://www.ara.cat/societat/canvi-climatic-cal-preparar-viure-menys-aigua_1_4449576.html.

Borer, B. *et al.* (2020) 'Reduced gravity promotes bacterially mediated anoxic hotspots in unsaturated porous media', *Scientific Reports*, 10(1), pp. 1–9. doi: 10.1038/s41598-020-65362-w.

Butler Jr., J. J. (2005) 'Hydrogeological Methods for Estimation of Spatial Variations in Hydraulic Conductivity', in Rubin, Y. and Hubbard, S. S. (eds) *Hydrogeophysics*. 1st edn. Springer Dordrecht, pp. 23–58. doi: 10.1007/1-4020-3102-5.

Butler Jr., J. J., McElwee, C. D. and Bohling, G. C. (1999) 'Pumping tests in networks of multilevel sampling wells: Motivation and methodology', *Water Resources Research*, 35(11), pp. 3553–3560. doi: 10.1029/1999WR900231.

Champ, D. R., Gulens, J. and Jackson, R. E. (1979) 'Oxidation-reduction sequences in ground water flow systems', *Canadian Journal of Earth Sciences*, 16(1), pp. 12–23. doi: 10.1139/e79-002.

Cho, M. S. *et al.* (2019) 'Field Trials of Chaotic Advection to Enhance Reagent Delivery', *Groundwater Monitoring and Remediation*, 39(3), pp. 23–39. doi: 10.1111/gwmr.12339.

Cooper Jr., H. H. and Jacob, C. E. (1946) 'A generalized graphical method for evaluating formation constants and summarizing well-field history', *Eos, Transactions American Geophysical Union*, 27(4), pp. 526–534. doi: 10.1029/TR027i004p00526.

Council Regulation (EU) 2020/741 on minimum requirements for water reuse, 2020. Official Journal, L177, 32-55.

Custodio, E. and Llamas, M. R. (1983) *Hidrología subterránea*. Barcelona: Editorial Omega.

Dillon, P. *et al.* (2019) 'Sixty years of global progress in managed aquifer recharge', *Hydrogeology Journal*, 27(1), pp. 1–30.

General Assembly declares access to clean water and sanitation is a human right (2010) *UN News*. Available at: https://news.un.org/en/story/2010/07/346122-general-assembly-declares-access-clean-water-and-sanitation-human-right (Accessed: 31 August 2020).

Gottlieb, J. and Dietrich, P. (1995) 'Identification of the permeability distribution in soil by hydraulic tomography', *Inverse Problems*, 11(2), pp. 353–360. doi: 10.1088/0266-5611/11/2/005.

Greskowiak, J. *et al.* (2006) 'Modeling seasonal redox dynamics and the corresponding fate of the pharmaceutical residue phenazone during artificial recharge of groundwater', *Environmental Science and Technology*, 40(21), pp. 6615–6621. doi: 10.1021/es052506t.

Gulev, S. K. *et al.* (2022) 'Changing State of the Climate System', in Masson-Delmotte, V. et al. (eds) *IPCC 2021: Climate Change 2021: The Physical Science Basis. Contribution of Working Group I to the Sixth Assessment Report of the Intergovernmental Panel on Climate Change*. Cambridge and New York: Cambridge University Press, pp. 287–422. doi: 10.1017/9781009157896.004.

Haberer, C. M. *et al.* (2012) 'Oxygen Transfer in a Fluctuating Capillary Fringe', *Vadose Zone Journal*, 11(3), p. vzj2011.0056. doi: 10.2136/vzj2011.0056.

Hui, I. and Cain, B. E. (2017) 'Overcoming psychological resistance toward using recycled water in California', *Water and Environment Journal*, 32(1), pp. 17–25. doi: 10.1111/wej.12285.

Jeffrey D Stanaway, Ashkan Afshin, Emmanuela Gakidou, Stephen S Lim, Degu Abate, Kalkidan Hassen Abate, C. A. (2018) 'Global, regional, and national comparative risk assessment of 84 behavioural, environmental and occupational, and metabolic risks or clusters of risks for 195 countries and territories, 1990–2017: a systematic analysis for the Global Burden of Disease Stu', *The Lancet*, 392, pp. 1923–94. doi: https://doi.org/10.1016/S0140-6736(18)32225-6.

Lester, D. R. *et al.* (2010) 'Scalar dispersion in a periodically reoriented potential flow: Acceleration via Lagrangian chaos', *Physical Review E - Statistical, Nonlinear, and Soft Matter Physics*, 81(4), pp. 1–11. doi: 10.1103/PhysRevE.81.046319.

Maliva, R. G. (2020) 'Soil-Aquifer Treatment', in *Anthropogenic Aquifer Recharge*.

Springer, Cham, pp. 623–645. doi: 10.1007/978-3-030-11084-0_19.

Martinez-Landa, L. *et al.* (2021) 'A methodology for the interpretation of aquifer tests: Application to CO_2 residual trapping experiments at the Heletz site', *International Journal of Greenhouse Gas Control*. Elsevier Ltd, 112, p. 103366. doi: 10.1016/j.ijggc.2021.103366.

Massmann, G. *et al.* (2006) 'The impact of variable temperatures on the redox conditions and the behaviour of pharmaceutical residues during artificial recharge', *Journal of Hydrology*, 328(1–2), pp. 141–156. doi: 10.1016/j.jhydrol.2005.12.009.

Meier, P. M., Carrera, J. and Sánchez-Vila, X. (1998) 'An evaluation of Jacob's method for the interpretation of pumping tests in heterogeneous formations', *Water Resources Research*, 34(5), pp. 1011–1025. doi: 10.1029/98WR00008.

Menegaki, A. N., Hanley, N. and Tsagarakis, K. P. (2007) 'The social acceptability and valuation of recycled water in Crete: A study of consumers' and farmers' attitudes', *Ecological Economics*, 62(1), pp. 7–18. doi: 10.1016/j.ecolecon.2007.01.008.

Neuman, S. P. (1987) 'Stochastic continuum representation of fractured rock permeability as an alternative to the REV and fracture network concepts', in Farmer, I. W. et al. (eds) *Rock Mechanics: Proceedings of the 28th U.S. Symposium, Tucson, AZ.* Rotterdam: A. A. Balkema, pp. 533–561.

OHCHR (2010) *Fact Sheet No. 35: The Right to Water*. Available at: https://www.ohchr.org/sites/default/files/2021-09/FactSheet35en.pdf.

Piscopo, A. N., Neupauer, R. M. and Mays, D. C. (2013) 'Engineered injection and extraction to enhance reaction for improved in situ remediation', *Water Resources Research*, 49(6), pp. 3618–3625. doi: 10.1002/wrcr.20209.

Rabadà, C. (2022) *El pantà de la Llosa del cavall al 30% de capacitat, La sequera del 22*. Available at: http://lasequera.cat/ (Accessed: 8 September 2022).

Reddy, K. R., D'Angelo, E. M. and Harris, W. G. (1998) 'Bio-geochemistry of wetlands', in Summer, M. E. (ed.) *Handbook of soil science*. Boca Raton: CRC Press, Inc., pp. 89–119. doi: 10.1201/9780203491454.

Ritchie, H. and Roser, M. (2017) *Water Use and Stress*, *OurWorldInData.org*. Available at: https://ourworldindata.org/water-use-stress (Accessed: 31 August 2022).

Rodríguez-Escales, P. *et al.* (2017) 'Improving degradation of emerging organic compounds by applying chaotic advection in Managed Aquifer Recharge in randomly heterogeneous porous media', *Water Resources Research*, 53, pp. 4376–4392. doi: 10.1002/2016WR020333.

Rolle, M. and Le Borgne, T. (2019) 'Mixing and Reactive Fronts in the Subsurface', *Reviews in Mineralogy and Geochemistry*, 85(1), pp. 111–142. doi: 10.2138/rmg.2018.85.5.

Sánchez-Vila, X. and Batista, E. (2009) 'Hidráulica de captaciones de agua', in Escuder, R. et al. (eds) *Hidrogeología*. First. Barcelona: FCIHS, pp. 314–377.

Survey, U. S. G. (2006) *Continued biodegradation of chloroethene compounds in ground water at operable unit 1, Naval Undersea Warfare Center, Division Keyport, Washington*. Available at: https://pubs.usgs.gov/sir/2006/5056/pdf/sir20065056.pdf.

Tartakovsky, A. M. (2010) 'Langevin model for reactive transport in porous media', *Physical Review E - Statistical, Nonlinear, and Soft Matter Physics*, 82(2), pp. 1–11. doi: 10.1103/PhysRevE.82.026302.

Theis, C. V. (1935) 'The relation between the lowering of the piezometric surface and rate and duration of discharge of a well using ground water storage', *Transactions of the American Geophysical Union*, 16(2), pp. 519–524. doi: 10.1029/TR016i002p00519.

Trabucchi, M., Carrera, J. and Fernàndez-Garcia, D. (2018) 'Generalizing Agarwal's method for the interpretation of recovery tests under non-ideal conditions', *Water Resources Research*, 54(9), pp. 6393–6407. doi: 10.1029/2018WR022684.

Trager, R. (2021) 'Long-anticipated plan to regulate PFAS chemicals unveiled in US', *Chemistry World*, October. Available at: https://www.chemistryworld.com/news/long-anticipated-plan-to-regulate-pfas-chemicals-unveiled-in-us/4014604.article.

UN-Habitat (2022) *World Cities Report 2022: Envisaging the Future of Cities*. Available at: https://unhabitat.org/sites/default/files/2022/06/wcr_2022.pdf.

UN-Water (2017) *The United Nations World Water Development Report 2017. Wastewater: The Untapped Resource, The United Nations World Water Development Report. Wastewater. The Untapped Resource*. Paris: UNESCO. Available at: http://unesdoc.unesco.org/images/0024/002471/247153e.pdf.

Valhondo, C. *et al.* (2014) 'Behavior of nine selected emerging trace organic contaminants in an artificial recharge system supplemented with a reactive barrier', *Environmental Science and Pollution Research*, 21(20), pp. 11832–11843. doi: 10.1007/s11356-014-2834-7.

Valhondo, C. *et al.* (2015) 'Characterizing redox conditions and monitoring attenuation of selected pharmaceuticals during artificial recharge through a reactive layer', *Science of the Total Environment*. Elsevier B.V., 512–513(C), pp. 240–250. doi: 10.1016/j.scitotenv.2015.01.030.

Valhondo, C. *et al.* (2020) 'Six artificial recharge pilot replicates to gain insight into water quality enhancement processes', *Chemosphere*, 240, p. 124826. doi: 10.1016/j.chemosphere.2019.124826.

Valhondo, C., Mart, L. and Wang, J. (2020) 'Reactive Barriers for Renaturalization of Reclaimed', *Water*, 12(4), p. 1012. doi: 10.3390/w12041012.

Water Reuse Europe (2018) *Water Reuse Europe: Review 2018*.

Yeh, T. C. J. and Liu, S. (2000) 'Hydraulic tomography: Development of a new aquifer test method', *Water Resources Research*, 36(8), pp. 2095–2105. doi: 10.1029/2000WR900114.